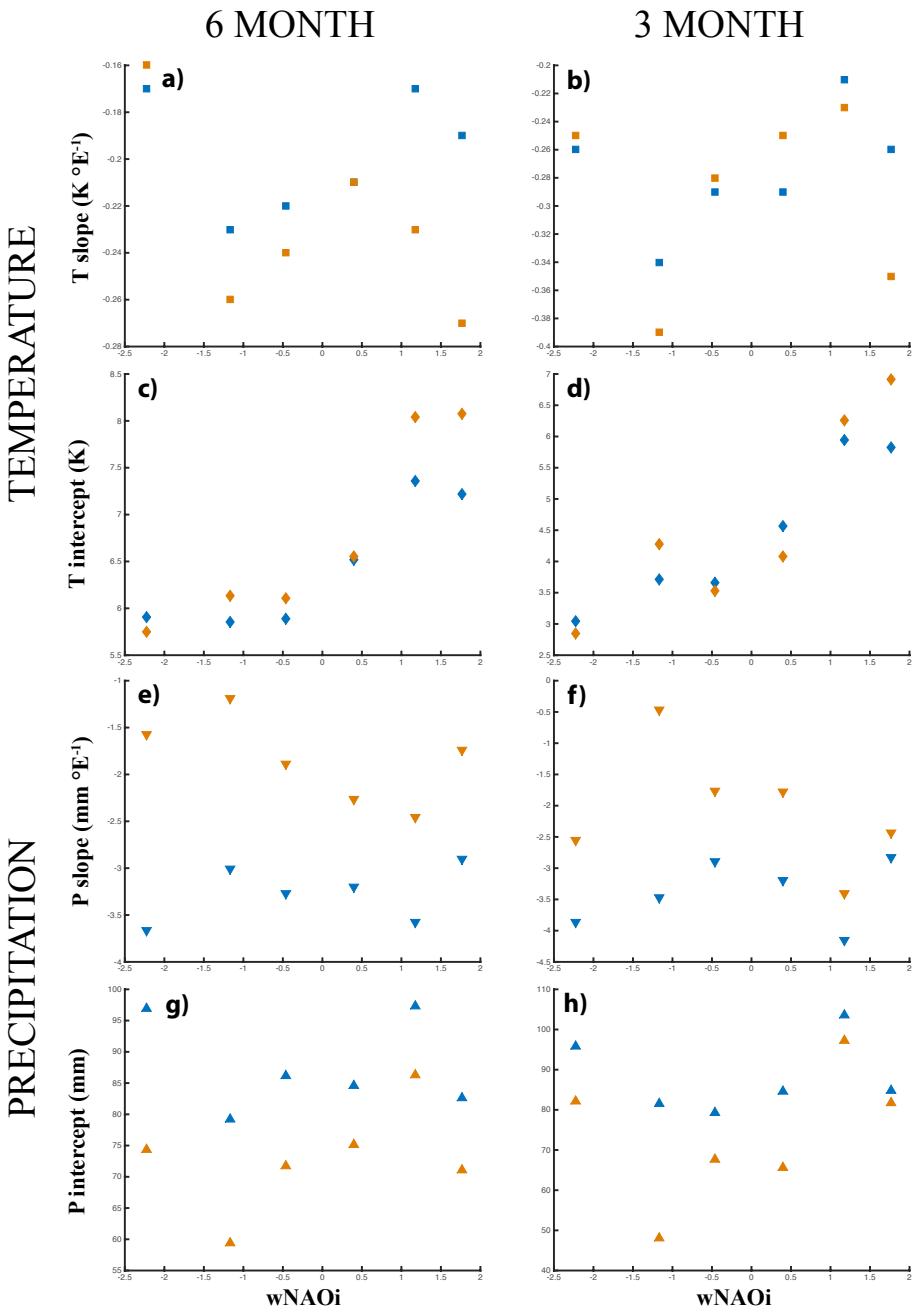

Blue symbols include all continental stations (as illustrated in Fig. 5); orange symbols indicate results where maritim stations are omitted.

Figure S1: Comparison of regression analysis for temperature (a-d) and precipitation (e-h) of all continental stations (blue symbols), illustrated in Fig. 5, and of the same compilation but with omitted maritime stations (station 1 and 2). The panels show the slopes (a, b, e, f) and intercepts (c, d, g, h) for the 6 month (left panels) and 3 month (right panels) winter period (periods are defined as stated in the manuscript). For the temperature results only small differences between the two compilations can be observed (a-d); for the 6 month compilation the T slope for very positive wNAOi classes is larger when maritime stations are omitted suggesting stronger temperature contrasts between central and eastern Europe. For the precipitation data the slopes of the reduced compilation of station data are smaller compared to the original compilation, however, the relationship to the wNAOi is not changed compared to the original compilation (e, f). The precipitation intercept is smaller for the reduced compilation compared to the original compilation, but as observed for the precipitation slopes, the NAO dependence for the

reduced compilation is similar as for the original compilation. In summary, the maritime stations (station 1 and 2) have only a negligible effect on the temperature results and change only the results of the precipitation data; however, the NAO dependence of the results is not changed and there are no shortcomings regarding the interpretation of the original dataset.

Multi-box exercise. The effect of the precipitation history on a longitudinal gradient, is illustrated in Figure S1 for $\delta^{18}O_P$ using a multi-box Rayleigh distillation model. The multi-box model is composed of 15 boxes. The initial $\delta^{18}O$ value of the atmospheric moisture in the 1st box is assumed to be -20 ‰. The $\delta^{18}O_P$ value and the $\delta^{18}O$ value of the atmospheric moisture of each box is calculated using the remaining amount of atmospheric moisture and its $\delta^{18}O$ value (transferred from the previous box), the respective amount of rainfall and the temperature at condensation using the standard Rayleigh equations for the mother and daughter products (Mook, 2006) and the isotope fractionation factor of Majoube (1971). The temperature and the amount of precipitation in every box is kept constant at 10 °C and 10 mm, respectively. To vary the amount of precipitable water Q_0 equates the sum of the total precipitation in all boxes and is multiplied by a factor that varies between 2.5 and 1.3. The higher the factor is the more moisture is left in the last box. The multi-box approach demonstrates that $\delta^{18}O_P$ values are more sensitive to the precipitation history f when the initial amount of precipitable water Q_0 is smaller. Similar results are obtained if instead of Q_0 the amount of precipitation is varied resulting in steeper longitudinal gradients if the amount of precipitation increases (not shown).

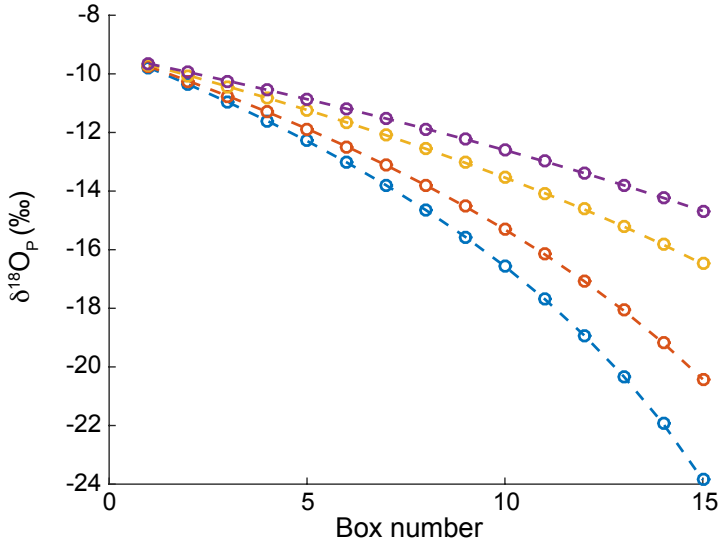

Figure S2: Multi-box exercise assuming a Rayleigh-type model for the condensation and associated isotope fractionation for precipitation $\delta^{18}OP$. The propagation of the $\delta^{18}O_P$ values through the boxes for different initial amounts of atmospheric moisture Q_0. Q_0 is determined in times of total precipitation of all boxes with a scaling factor of 1.3 (blue), 1.5 (orange), 2 (yellow) and 2.5 (purple) showing that the $\delta^{18}O_P$ values along the transect (from box to 1 to 15) becomes more depleted the smaller Q_0 is. Therefore, a longitudinal transect of $\delta^{18}O_P$ (and δD_P) values is more sensitive to the precipitation history, in terms of the isotope depletion in rare ^{18}O and ^{2}H isotopes along a longitudinal gradient when Q_0 is smaller resulting in steeper longitudinal $\delta^{18}O_P$ (and δD_P) gradients, i.e., increasing gradient slopes.

ECHAM5-wiso simulations

Data and methods (ECHAM5-wiso): To independently evaluate possible mechanisms that determine the longitudinal $\delta^{18}O_{pw}$ and δD_{pw} gradients, the $\delta^{18}O_{pw}$ and δD_{pw} data from the isotope-enabled General Circulation Model ECHAM5-wiso (Langebroek et al., 2011;Werner et al., 2011) were analysed for the period 1960-2010 AD. The analysed ECHAM5-wiso model output has a spatial resolution of 1.9°x1.9°.

(Details on the ECHAM5-wiso model and the ECHAM5-wiso data NAO-dependence are given by Werner et al. (2011) and Langebroek et al. (2011) respectively). To compare the ECHAM5-wiso data with the station-based data shown in the manuscript, only the model output for those grid cells were analysed where a continental station is located (Figure 1). For these selected grid cells, the 3-month (December-February) and 6-month (October-March) $\delta^{18}O_{pw}$ and δD_{pw} values were calculated. These model winter values were grouped (as described in Section 2.1) using the ECHAM5-wiso winter NAO index. The monthly ECHAM5-wiso NAO index is calculated by Principal Component Analysis (PCA) from the model monthly sea level pressure field in the sector from 40 °W to 40 °E and 20 °N to 80 °N (see Langebroek et al., 2011 for details on the calculation of the ECHAM5-wiso NAO index). The ECHAM5-wiso winter NAO index is the mean NAO index for the months December to March. For every grid cell, this approach results in six median $\delta^{18}O_{pw}$ and δD_{pw} (one median value for every NAO class) of which the model longitudinal $\delta^{18}O_{pw}$ and δD_{pw} gradient is calculated.

Results (ECHAM5-wiso): The longitudinal $\delta^{18}O_{pw}$ and δD_{pw} gradients that result from the ECHAM5-wiso simulations are shown in Figure 4 and Figure S3 (Figure S3 is the same as Figure 4 but is shown here again for simplicity).

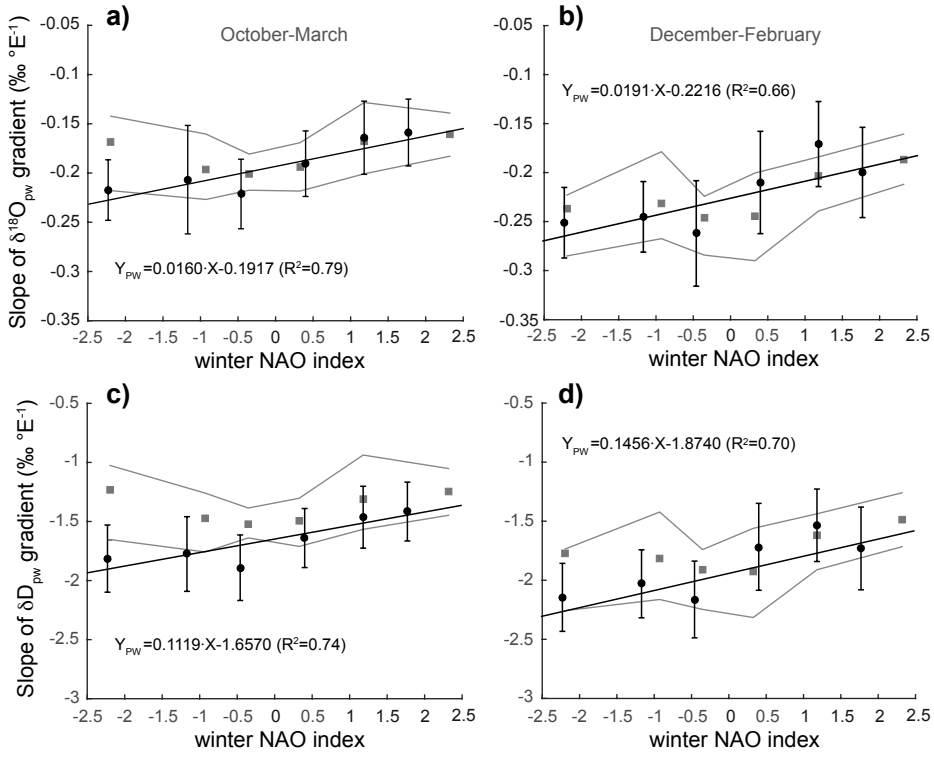

Figure S3: Illustration of the slopes of the $\delta^{18}O_{pw}$ (a and b) and δD_{pw} (c and d) longitudinal gradients across Europe (filled circles) – and their respective standard errors – calculated from 13 continental GNIP stations for the 6-month (October-March) (a and c) and 3-month (December to February) (b and d) winter period. More negative wNAOi classes result in a steeper isotope gradient across Europe in winter and, therefore, more strongly depleted $\delta^{18}O_{pw}$ and δD_{pw} values with increasing distance (towards the east) from the European western margin. The coefficient for the linear regression between the observed slopes and the class of the wNAOi is 0.016±0.004 (r^2=0.79; p<0.05) for Fig. 1a, 0.019±0.006 (r^2=0.65; p=0.0502) for Fig. 1b; 0.111±0.033 (r^2=0.74, p<0.05) for Fig. 1c and 0.146±0.048 (r^2=0.70, p<0.05) for Fig 1d (units are ‰ °E^{-1}/wNAOi). These equations state the results from the linear regression where Y_{PW} is the slope of the $\delta^{18}O_{pw}$ or δD_{pw} gradient and X is the wNAOi. The filled grey squares show the median slopes of the ECHAM5-wiso simulations; the grey envelope indicates the 25% and 75% quantiles of the ECHAM5-wiso slopes. The regression analysis of the median slopes of the ECHAM5-wiso $\delta^{18}O_{pw}$ or δD_{pw} gradients reveals that only the 3 month averages have a considerable R^2 value (but still quite high p-values) while the

6 month values have an almost absent linear correlation to the wNAOi class: results for $\delta^{18}O_{pw}$, r^2=0.19, p>0.1 (6 month), r^2=0.62, p=0.06 (3 month); for δD_{pw}, r^2=0.02, p>0.1 (6 month), r^2=0.40, p>0.1 (3 month).

The comparison of the station-based slopes of the longitudinal $\delta^{18}O_{pw}$ and δD_{pw} gradients for the different wNAOi classes with the ones from the ECHAM5-wiso simulations show that modelled slopes fit in principle the observational results (Figure S3). However, in contrast to the observational data, the modelled slopes have no clear relationship the wNAOi classes. Only the results of the 3-month $\delta^{18}O_{pw}$ values reveal a slight correlation (p=0.06) (see regression results in Figure S3). In summary, the range of the modelled slopes of the longitudinal $\delta^{18}O_{pw}$ and δD_{pw} gradients cover the station-based results, however, their dependence on the wNAOi is much smaller compared to the observational data.

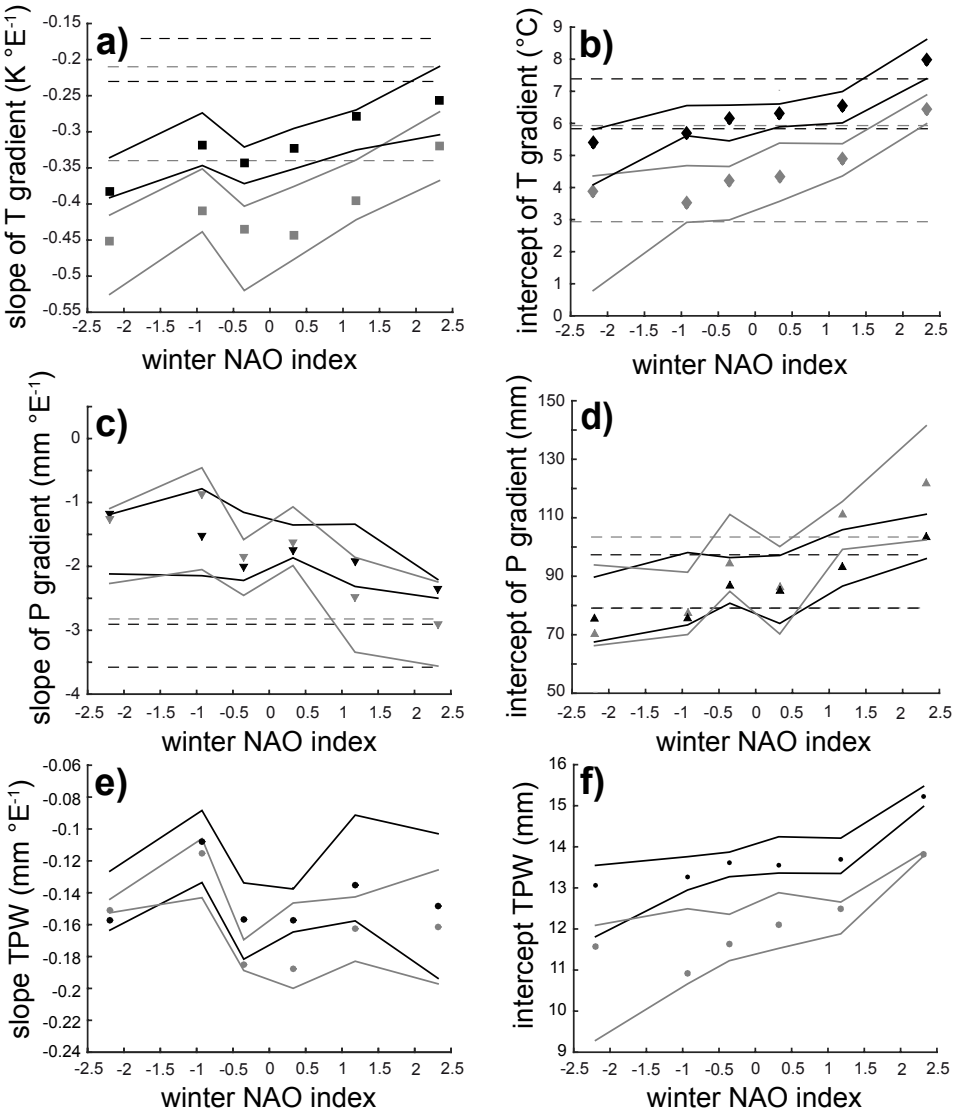

Figure S4: ECHAM5-wiso outputs: The six panels illustrate the median slope of the gradient for a) temperature (T), c) precipitation (P) and e) the total precipitable water (TPW) depending on the class of the wNAOi from the analysed ECHAM5-wiso grid cells. Panel b), d) and f) shows the median intercept of the linear regression for the temperature, precipitation and total precipitable water gradient versus the class of wNAOi. The envelopes (straight line) indicate the 25% and 75% quantile. Back colours indicate the results for the 6-month winter period and grey colours the results from 3-month winter period. The dashed lines in panel a) to d) indicate the observed variability of these parameters derived from the observational datasets from the GNIP stations as illustrated in Figure 5.

To better access this different behaviour we have evaluated the temperature and precipitation of the ECHAM5-wiso simulations and their dependence on the ECHAM5-wiso wNAOi from the relevant ECHAM5-wiso model grid cells. Furthermore, the total precipitable water was analysed for the ECHAM5-wiso dataset. These variables were also grouped according to wNAOi class of their respective winters, and the median of temperature and precipitation were calculated for each wNAOi class (Figures S4 and S5).

Similar temperature-NAO relationships are observed for the ECHAM5-wiso simulations, with increasingly steeper model air temperature gradients and a smaller temperature intercept for lower wNAO indices (Figure S4a and S4b). However, in comparison with the slopes derived from the GNIP datasets, the slopes derived from the ECHAM5-wiso simulations suggest steeper temperature gradients (Figure S4a). The intercept of the temperature regression derived from the ECHAM5-wiso simulations is similar to that from the observational datasets (Figure S4b). Therefore, the longitudinal temperature gradients of the ECHAM5-wiso simulations suggest comparable temperatures at 0°E (the temperature intercept), but much cooler temperatures in eastern Europe (a steeper temperature slope) compared with the observed air temperatures in the GNIP datasets. This results in much greater temperature related isotope fractionation effects compared to the observational data as explained in the following.

By contrast with the observational (GNIP) data discussed in the manuscript, the ECHAM5-wiso simulated differences in $\delta^{18}O_{pw}$ and δD_{pw} can largely be accounted for by model air-temperature differences alone. Only for the most negative winter NAO class does the expected temperature-driven west to east change in $\delta^{18}O_{pw}$ and δD_{pw} exceed the ECHAM5-wiso simulated differences derived from slope of the lowest wNAOi class. If the slope of the ECHAM5-wiso longitudinal $\delta^{18}O_{pw}$ and δD_{pw} gradients were driven by winter air temperature gradients alone, the average temperature sensitivity for the remaining five wNAOi classes for the 6-month winter period for $\delta^{18}O_{pw}$ and δD_{pw} calculated from the ECHAM5-wiso simulations varies between 0.59 and 0.63 ‰/K for $\delta^{18}O_{pw}$ and 4.44 and 4.87 ‰/K for δD_{pw}. For the 3-month winter period, equivalent temperature sensitivities from the ECHAM5-wiso simulations range between 0.51 and 0.58 ‰/K for $\delta^{18}O_{pw}$ and 4.09 and 4.65 ‰/K for δD_{pw} and are smaller compared to the 6-month winter period. Hence, the temperature sensitivities for $\delta^{18}O_{pw}$ and δD_{pw} derived from the ECHAM5-wiso are apparently somewhat lower compared to the theoretically estimated ones based on the approach of Dansgaard (1964). One explanation for the larger temperature sensitivities derived by the Dansgaard (1964) approach may be that the initial temperature at which the moisture condensation begins in the atmosphere is actually greater than 0°C as assumed in our theoretical calculations. Higher condensation temperatures are reasonable considering that the temperature intercepts derived from the observed temperatures vary between c. 3 °C and 7 °C (Figure 5b).

In the ECHAM5-wiso simulations, a clear relationship exists between the slope and intercept of the longitudinal precipitation gradient (Figure S4c and S4d). The slopes, as well as the intercepts of the precipitation gradients are smaller for lower wNAOi classes, suggesting that the west-east difference of the amount of precipitation decreases (increases) for lower (higher) wNAOi classes in the model. Furthermore, the decreasing (increasing) intercept of the precipitation gradient for lower (higher) wNAOi classes suggests a lower (higher) amount of rainfall in the western grid cells. Analysis of the total amount of precipitation for all grid cells reveals lower values for the total amount of rainfall in the selected grid cells (i.e. the sum of precipitation from all grid cells) for lower wNAOi classes. For the 6-month winter period, for example, the median of the total precipitation decreases from 1091 mm for the highest wNAOi class to 852.5 mm for the lowest wNAOi class. In the case of the 3-month winter period, the median of the total precipitation decreases from 1270 mm to 800 mm from the highest to the lowest wNAOi class. For the lowest wNAOi class, the total amount of precipitation of all grid cells is about 78 % and 63 % of that from the highest wNAOi class for the 6-month and 3-month winter periods, respectively. Thus, the ECHAM5-wiso output is not consistent with the observed data for precipitation at the GNIP stations, which show only a very weak relationship with the wNAOi class (R^2=0.07). Indeed, in the observational data, the total amount of precipitation for the lowest wNAOi class is actually marginally higher compared with that for the highest wNAOi class (c. 762 mm compared to 866 mm for the 6-month winter period, and c. 797 mm compared to 830 mm for the 3-month winter period). This comparison indicates that the precipitation

history inferred from the observational datasets and the ECHAM5-wiso simulations are quite different. The effect of these differences on the longitudinal $\delta^{18}O_{pw}$ and δD_{pw} gradients are discussed below.

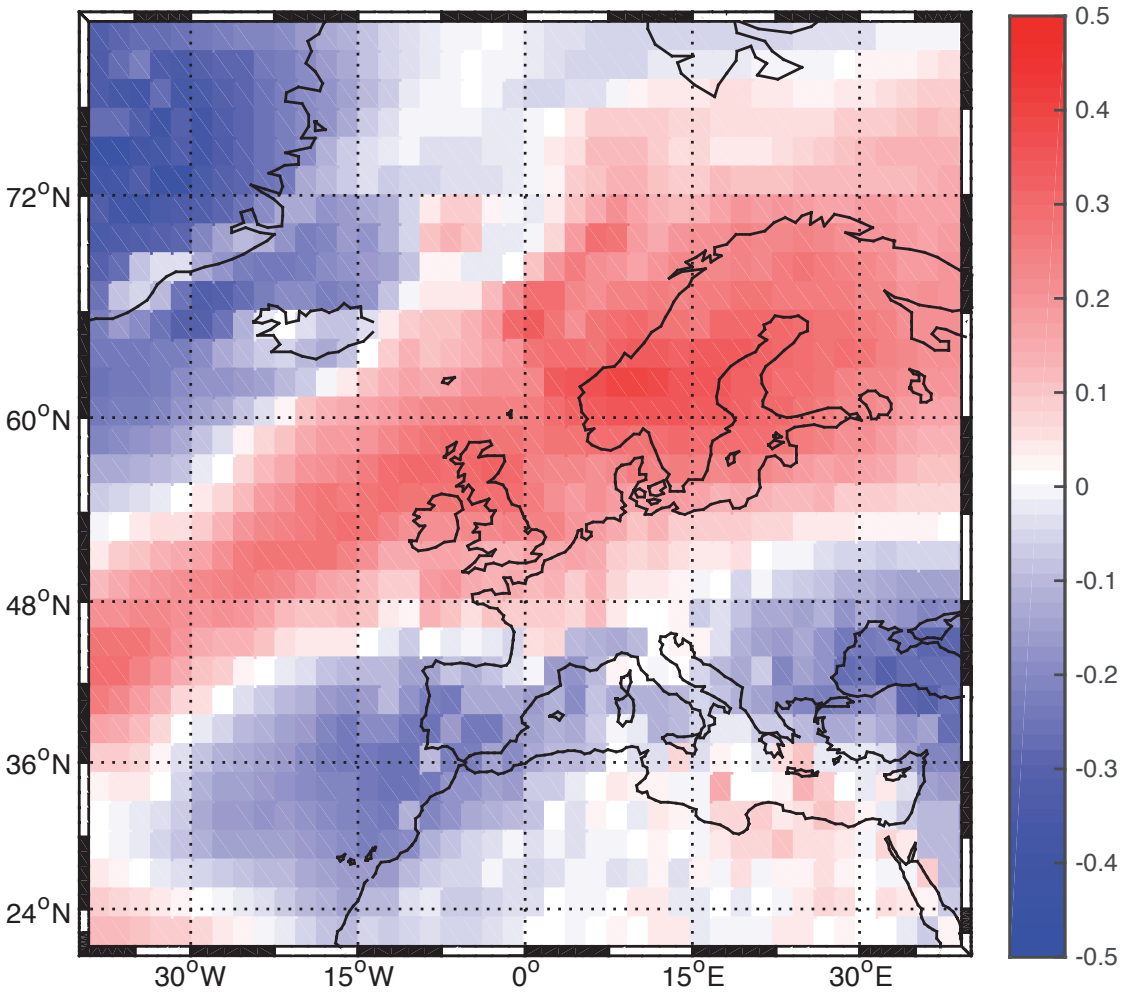

Figure S5: Correlation map between the monthly index of the North Atlantic Oscillation and the amount of total precipitable water for the month from December to March derived from ECHAM5-wiso simulation. The map shows the sector from 20°N to 80°N and from 40°W to 40°E for the years from 1960 to 2010 AD (see text for details on the ECAHM5-wiso simulations). The colour bar on the right side indicates the colour code for the correlation coefficients.

The relationship between ECHAM5-wiso total precipitable water (TPW) and the wNAOi reveals a similar pattern as observed for the NCEP/NCER reanalysis dataset (cf. Figure 6) and described by (Trigo et al., 2002): a tripol-like pattern with negative correlations coefficients between TPW and the wNAOi over southeast Greenland and the Mediterranean region (including the Iberian Peninsula) and positive correlation coefficients over central and northern Europe (Figure S5). Analyses of the ECHAM5-wiso TPW gradients based on TPW data from grid cells where continental stations are located indicates that the slope of the TPW gradients has no relationship to the class of the wNAOi while the intercept of the TPW gradient has a clear relationship to the wNAOi. The intercept of the ECHAM5-wiso TPW gradients is higher for more positive wNAOi classes and vice versa, which is in agreement with the analyses of the NCEP/NCER reanalysis dataset. Compared with the amount of precipitable water for the highest wNAOi class, the atmosphere contains only about 85.7 % for the lowest wNAOi class for the 6-month winter period for example. In the ECHAM5-wiso simulations, the total amount of precipitation (78 % for the 6-month winter period) decreases more along the longitudinal transect than does the amount of precipitable water. As a result, the precipitation history f becomes less sensitive to the rainout history along the longitudinal

gradient for lower wNAOi classes. The differences between the theoretically derived temperature sensitivity by Dansgaard (1964) and the temperature sensitivity derived by the ECHAM5-wiso simulations could thus be ascribed to the changing ratio of total precipitation and amount of precipitable water as seen in the ECHAM5-wiso simulations. For the *ECHAM5-wiso*, air temperature gradients are clearly the most important factor that controls the longitudinal $\delta^{18}O_{pw}$ and δD_{pw} gradients, In *ECHAM5-wiso*, the precipitation history seems to be of relatively minor importance, because changes in the amount of precipitable water are mediated by changes in the simulated amount of precipitation. The reason for the different strength of these two mechanisms (temperature gradient and precipitation history) on the longitudinal $\delta^{18}O_{pw}$ and δD_{pw} gradients for the observed (GNIP) and simulated (ECHAM5-wiso) datasets remains unclear, suggesting that the ECHAM5-wiso simulations warrant further investigation.

Supplementary discussion on the mechanisms that control the $\delta^{18}O_{pw}$ and δD_{pw} of the Mediterranean stations. There are clear relationships (for the 3-month and 6-month winter period) of temperature ($r>0.5$) and precipitation ($r<-0.5$) to the wNAOi as well as between these two parameters and $\delta^{18}O_{pw}$ and δD_{pw} ($r>0.5$ for temperature and $r<-0.4$ for precipitation) from the station Avignon suggesting that temperature and precipitation are important parameter that control $\delta^{18}O_{pw}$ and δD_{pw}. For Zagreb in contrast the controlling mechanism for the observed strong NAO-relationship remain unclear. For the 3-month dataset there is a NAO-relationship to temperature ($r>0.45$) and precipitation ($r<-0.5$) but this is clearly absent for the 6-month dataset. Similar relationships between temperature and precipitation and the $\delta^{18}O_{pw}$ and δD_{pw} datasets as for Avignon are observed for the 3-month dataset ($r>0.3$ for temperature and $r<-0.4$ for precipitation). For Locarno a NAO-relationship is found for the temperature ($r>0.45$) as well as the precipitation ($r<-0.33$) for both the 3-month and 6-month winter period. For $\delta^{18}O_{pw}$ only a relationship to the temperature is observed ($r>0.5$) while there is a relationship between δD_{pw} and temperature ($r>0.4$) and precipitation ($r>0.45$). For the temperature and precipitation datasets from Genoa (Setri) only the precipitation has a relationship to the wNAOi ($r<-0.4$). However, there are no relationships observed between temperature and precipitation and the $\delta^{18}O_{pw}$ and δD_{pw} datasets; only the 3-month δD_{pw} dataset has a relationship to the temperature ($r=0.38$).

Supplementary data. The left panels show the box plots for the 6 months (October to March) and the right panels for the 3 months (December to February) winter season. The upper panels illustrate the $\delta^{18}O_{pw}$ values and the lower panels the δD_{pw} values. Every box plot illustrates the statistical variables (median, min, max, 25 and 75% quantile) for every wNAOi class from lowest to highest (left to right). Note that for some stations no data was available for NAO classes; in these cases the statistical results are only illustrated for the classes where data was collected (e.g. Station 15, Bern). For the individual wNAOi classes, the red line illustrates the median of the compilation of data; the edges of the blue rectangles marks the 25% and 75% quantile; the black bars illustrates the minimum and maximum value and the red plus sign pictures outliers (maximum whisker length is 1.5). (The figures were plotted using the MATLAB® function "boxplot".)

Station 1: Valentia (OBSERVATORY)

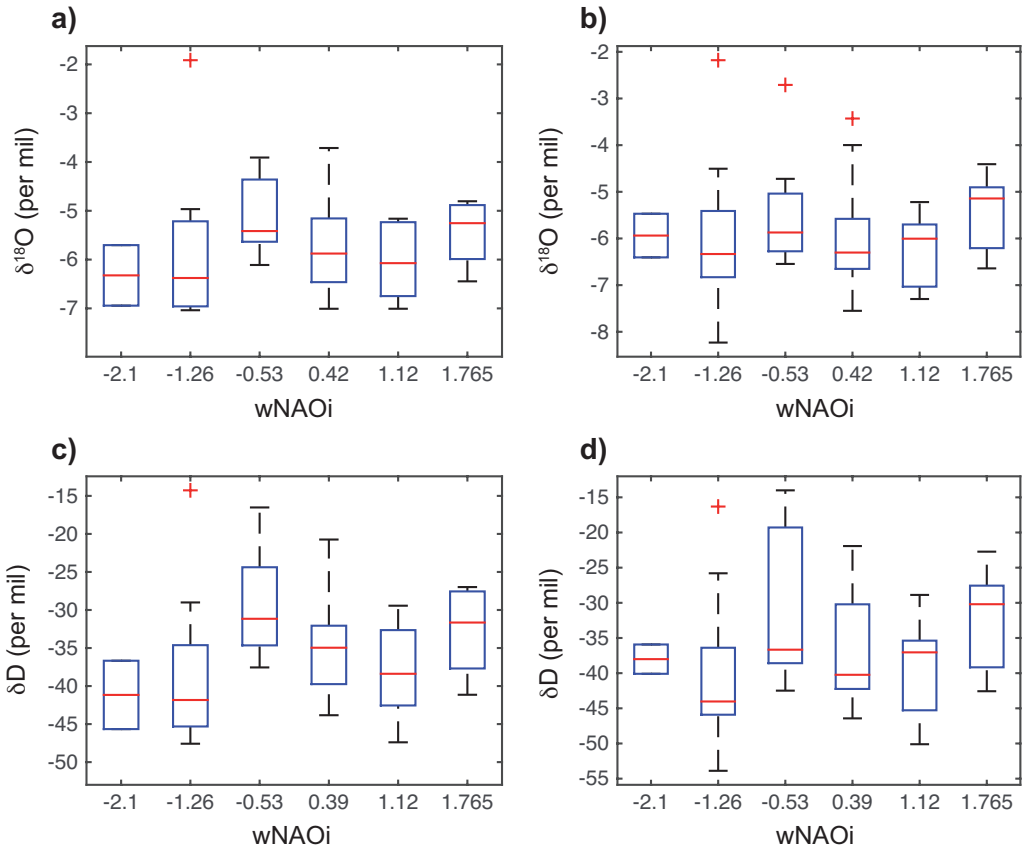

Figure caption exemplary given for the Valentia (OBSERVATORY): box plot (as described above) for the 6 months winter season (October to March) a) $\delta^{18}O_{pw}$ and c) δD_{pw} values and for the 3 months winter season (December to February) b) $\delta^{18}O_{pw}$ and d) δD_{pw} values for the various wNAOi classes sorted from the lowest (left) to the highest (right) wNAOi class. The red line illustrates the median; the edges of the blue rectangles marks the 25% and 75% quantile; the black bars illustrates the minimum and maximum value and the red plus sign pictures outliers.

Station 2: Wallingford

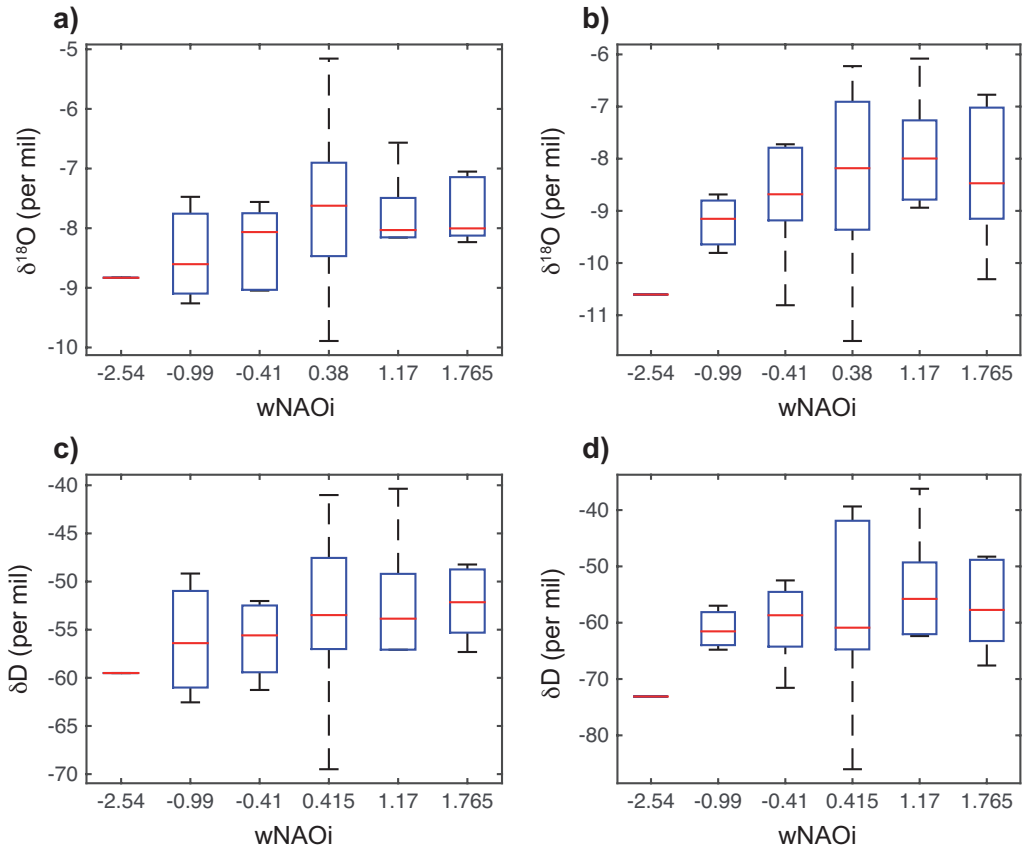

Station 3: Groningen

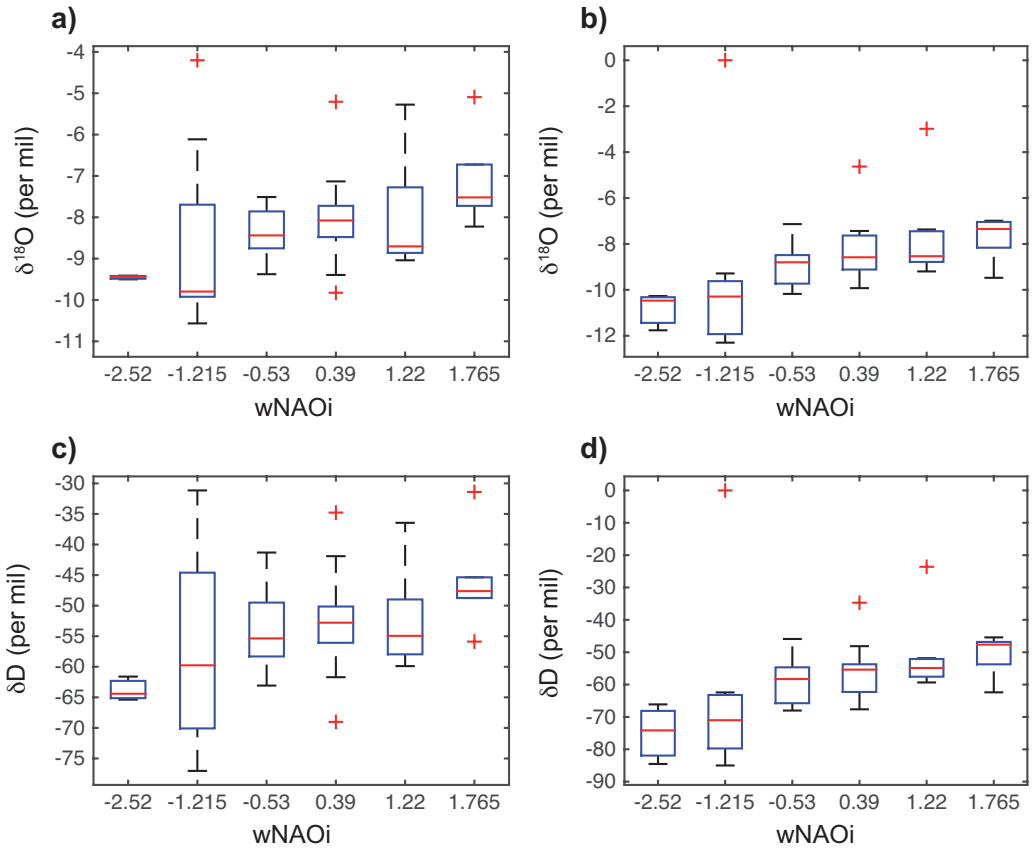

Station 4: Koblenz

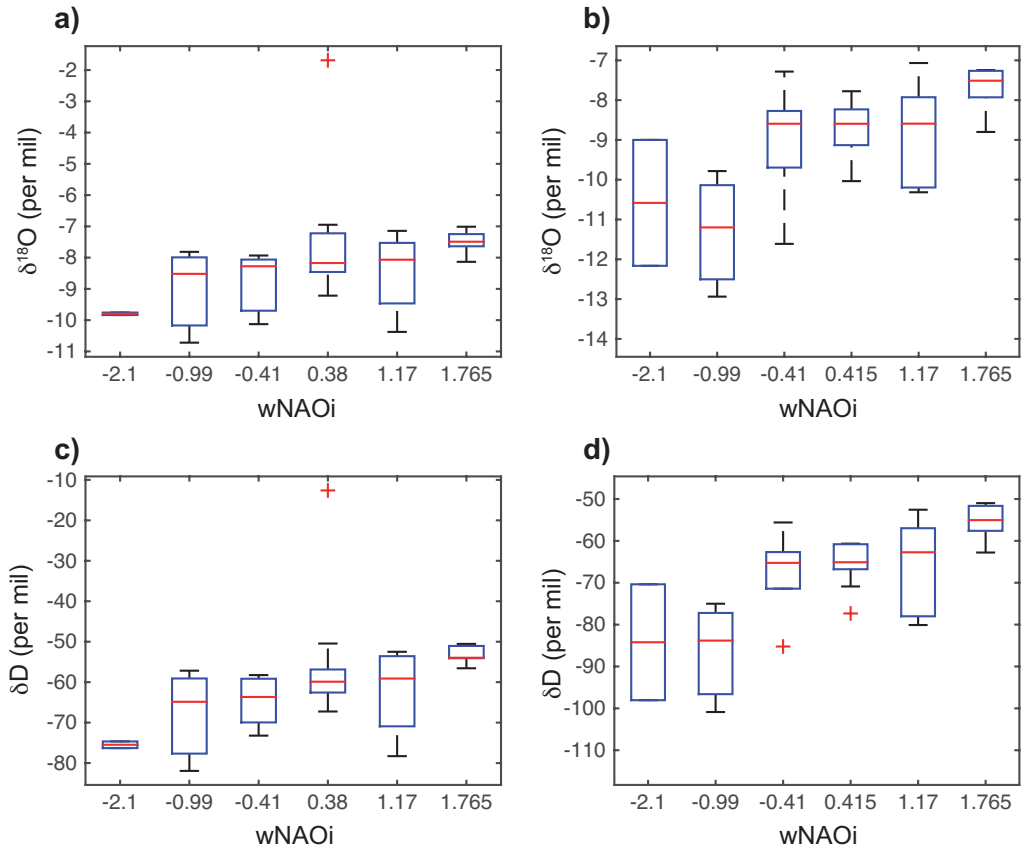

Station 5: Karlsruhe

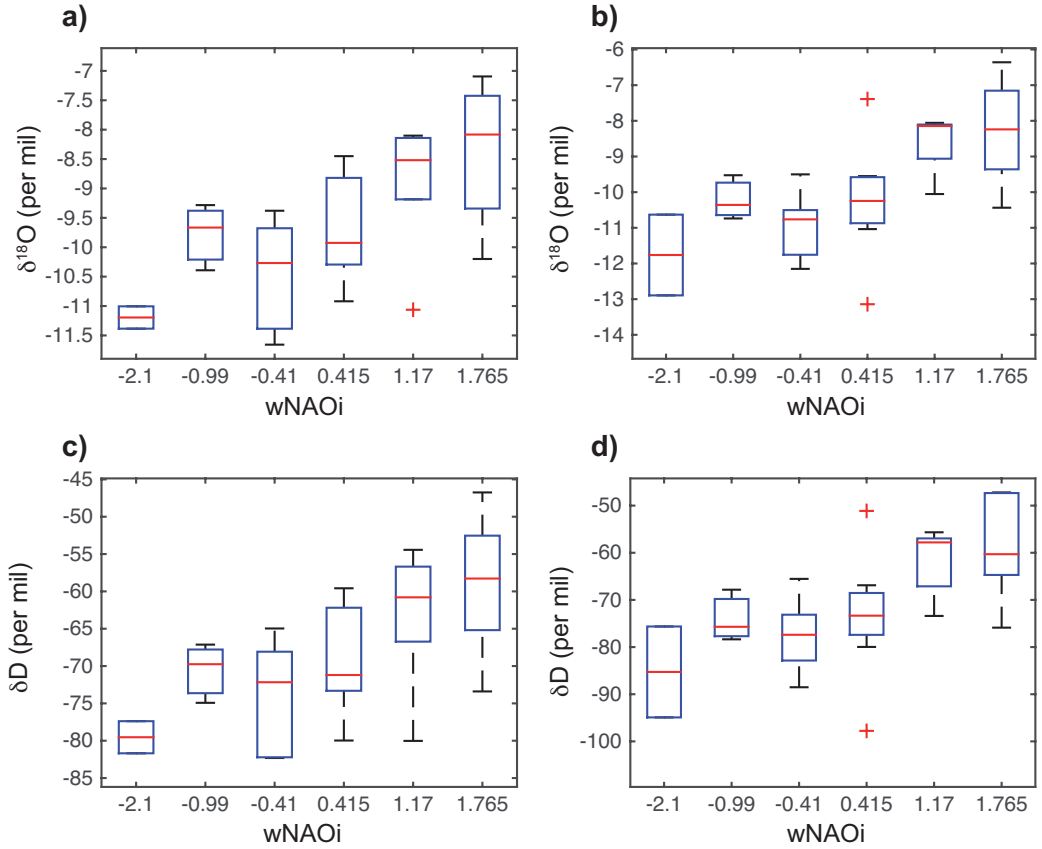

Station 6: Cuxhaven

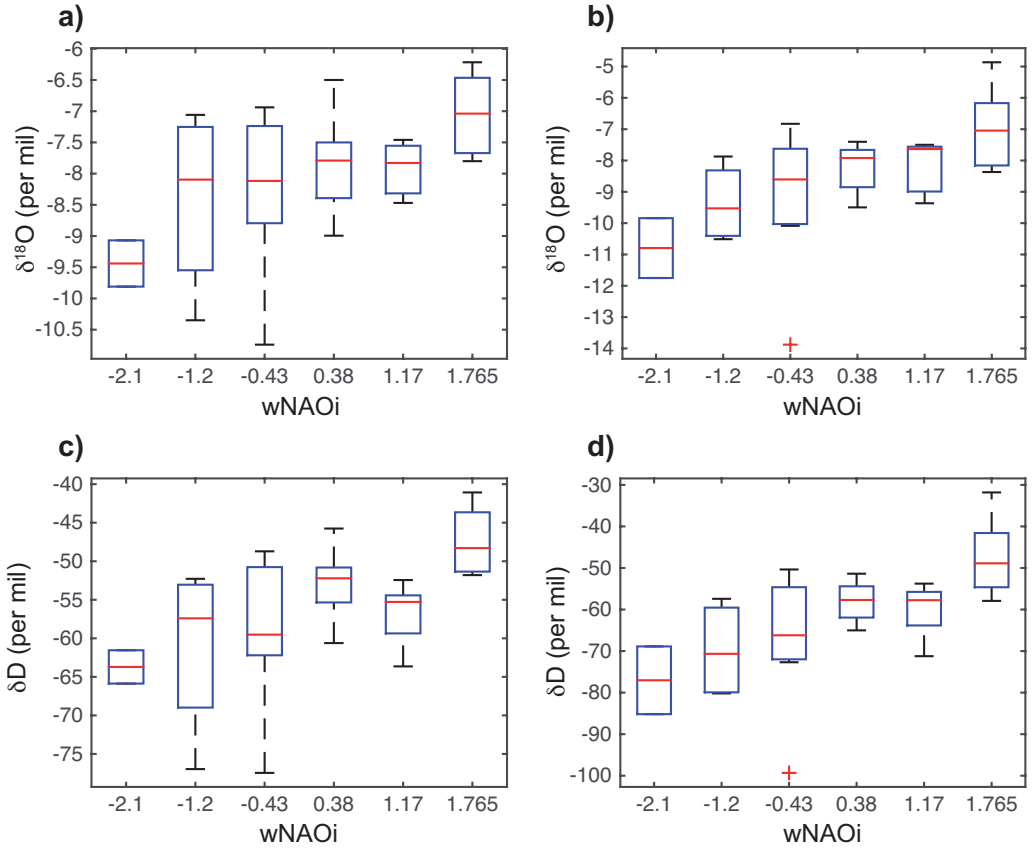

Station 7: Bad Salzuflen

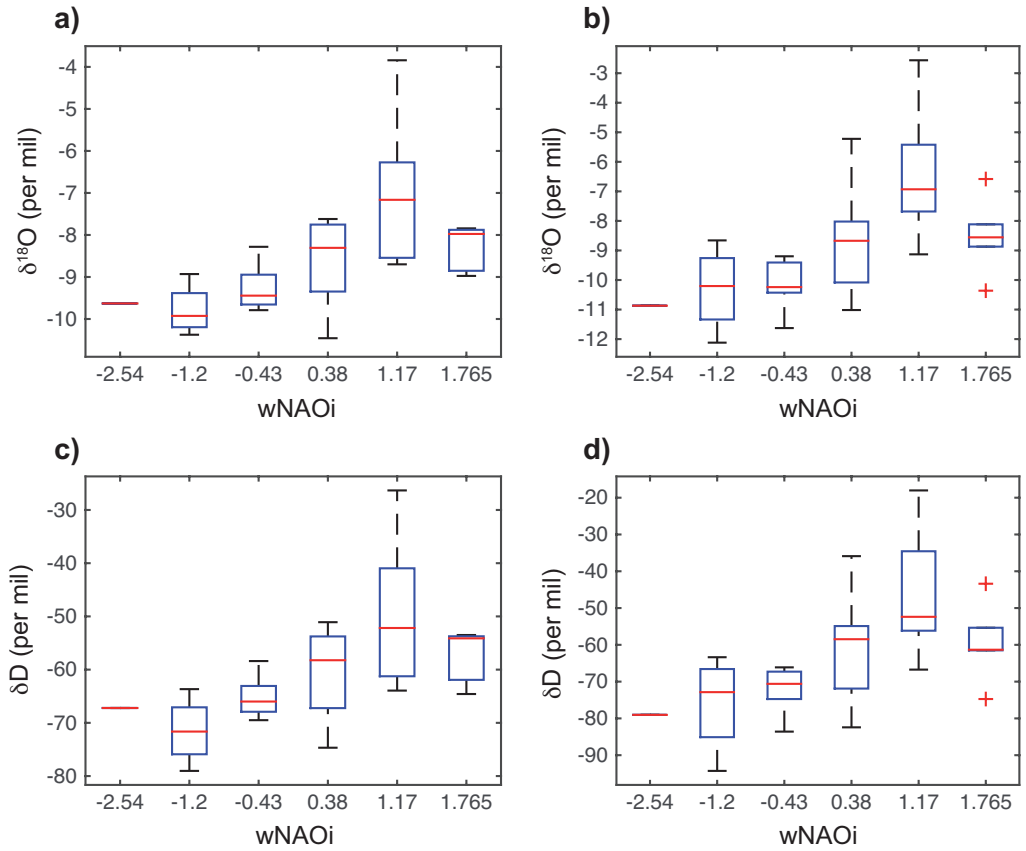

Station 8: Stuttgart (CANNSTATT)

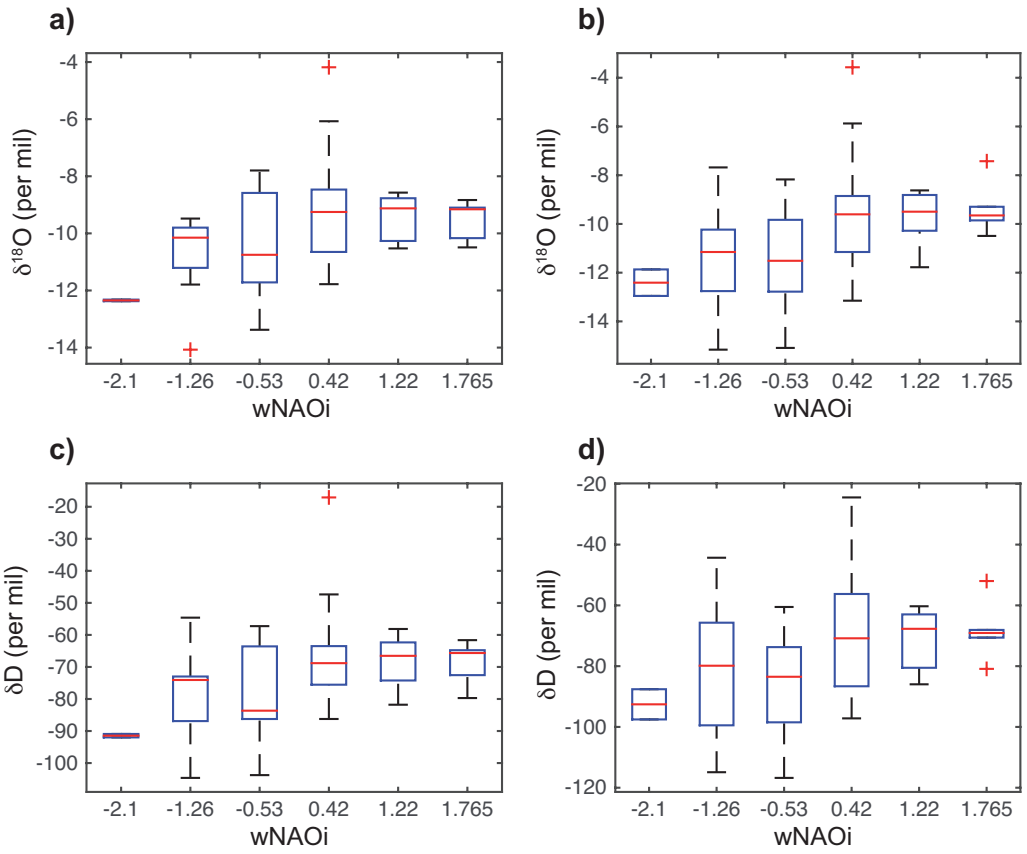

Station 9: Wuerzburg

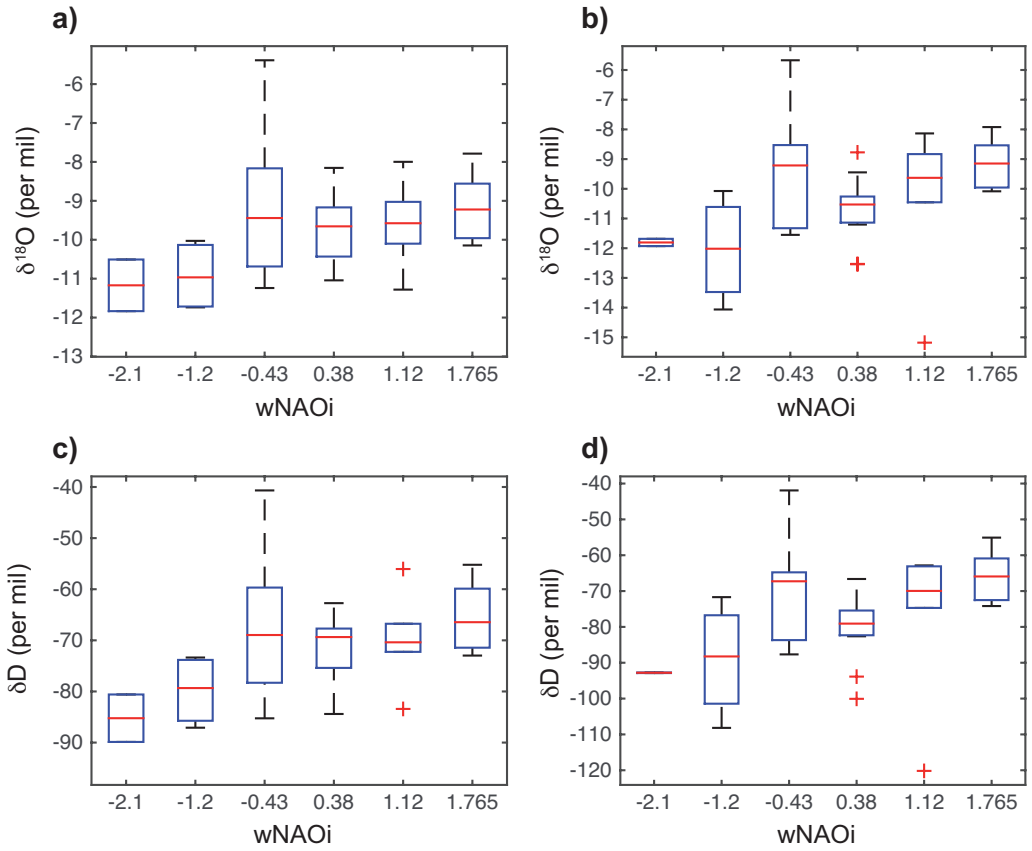

Station 10: Braunschweig

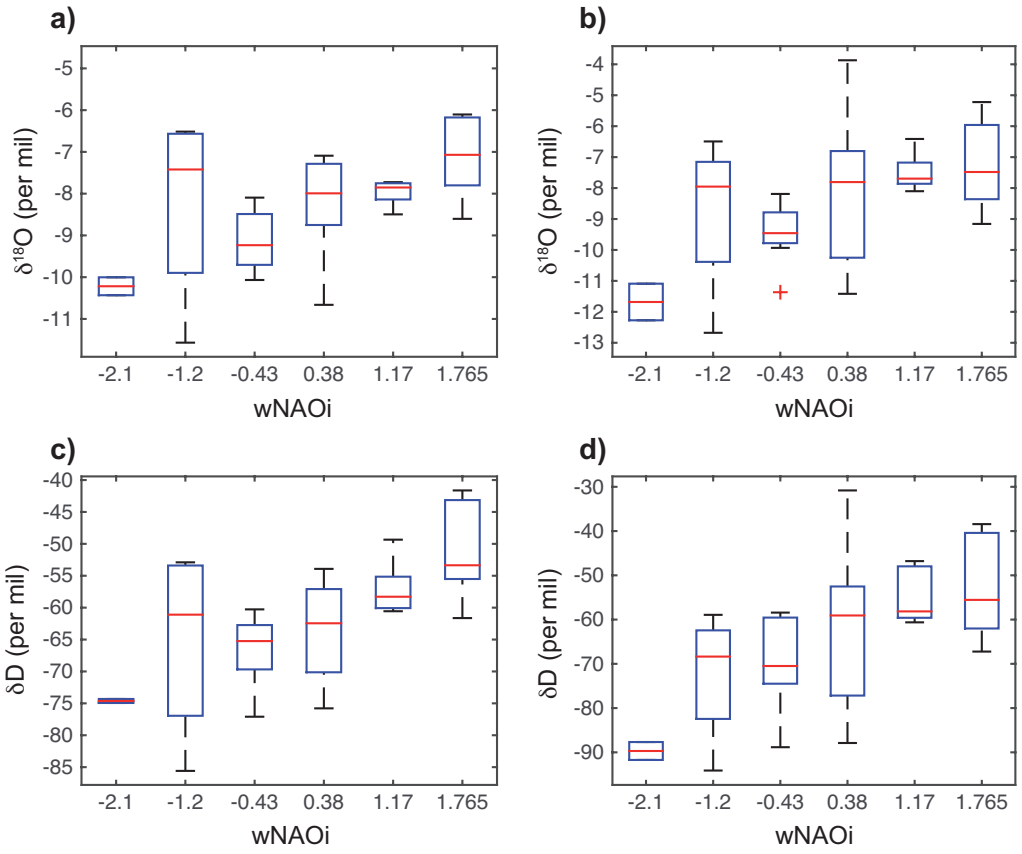

Station 11: Berlin

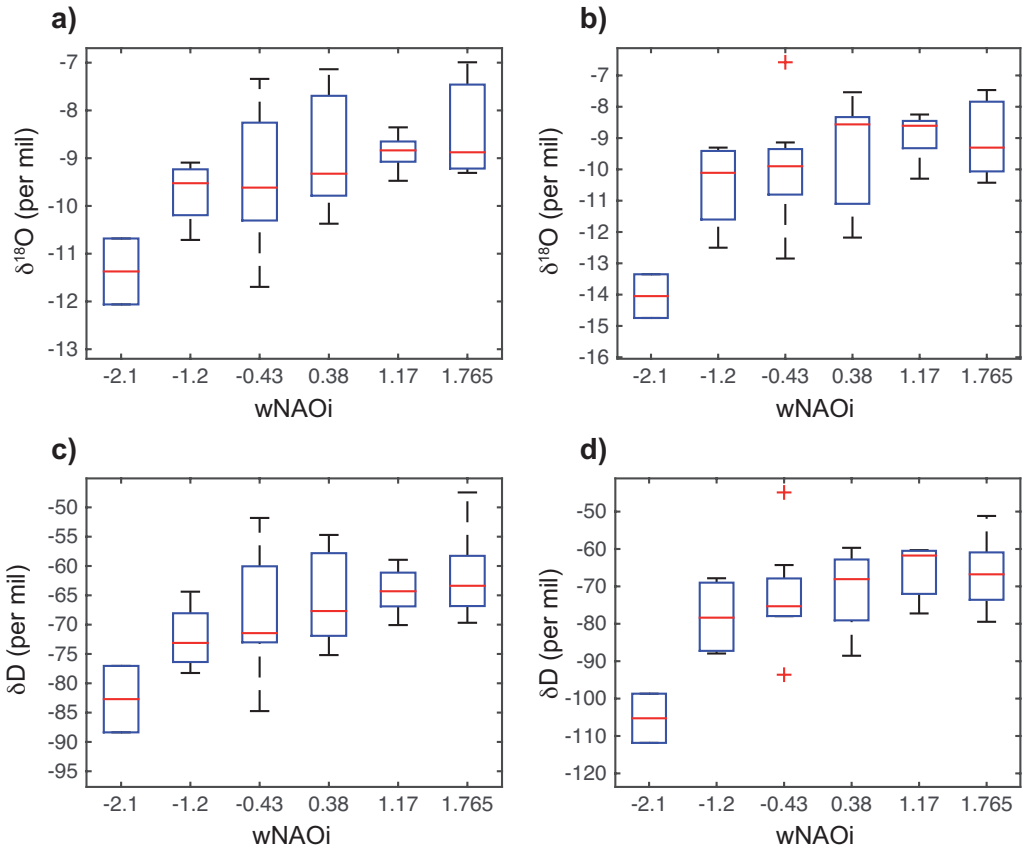

Station 12: Vienna (HOHE WARTE)

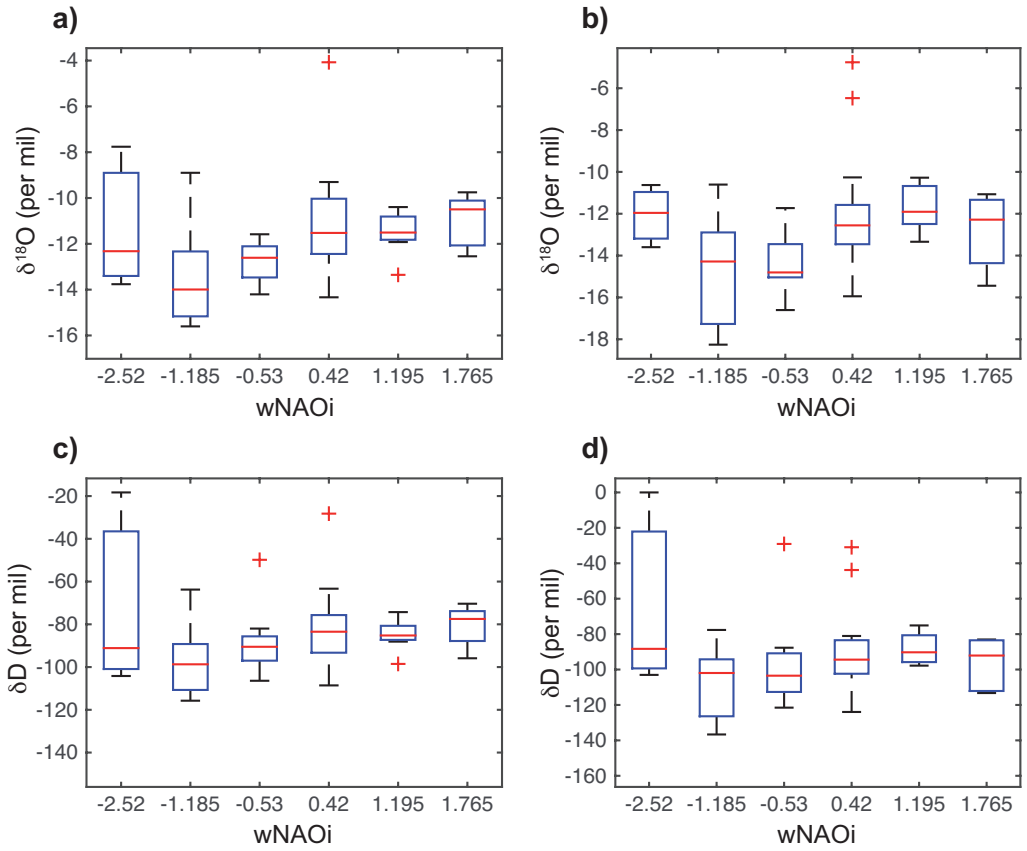

Station 13: Krakow (WOLA JUSTOWSKA)

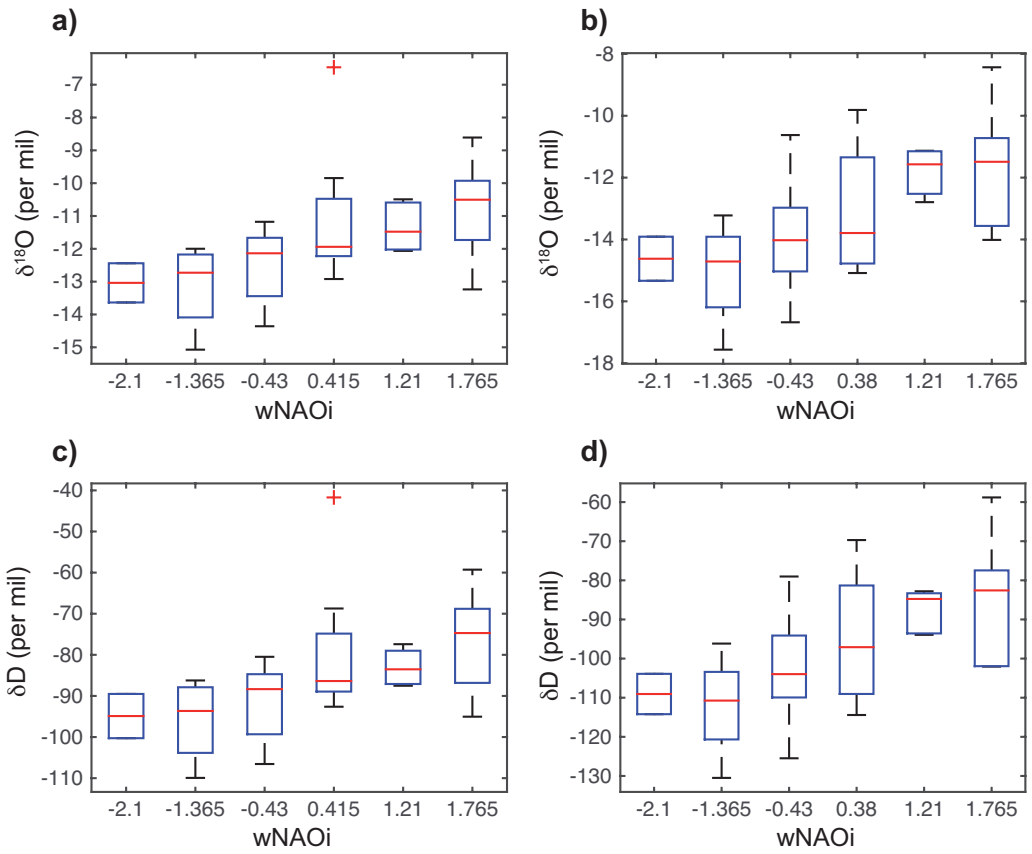

Station 14: Thonon-Les-Bains

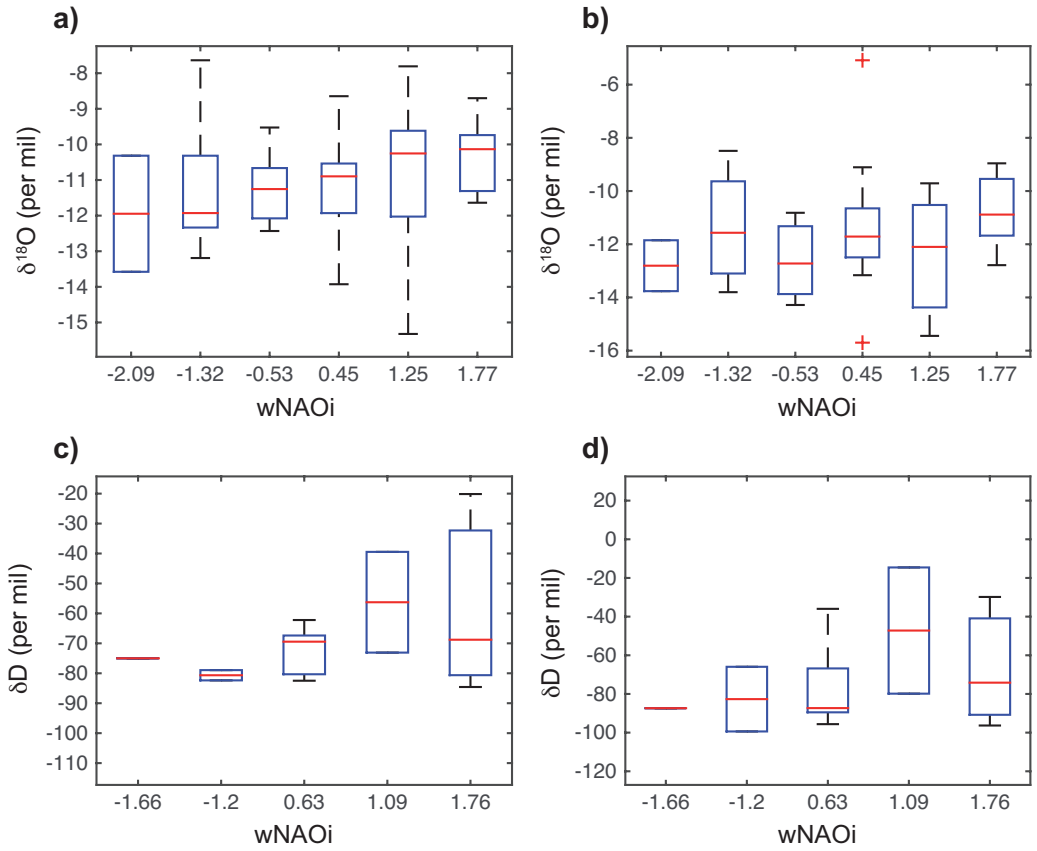

Station 15: Bern

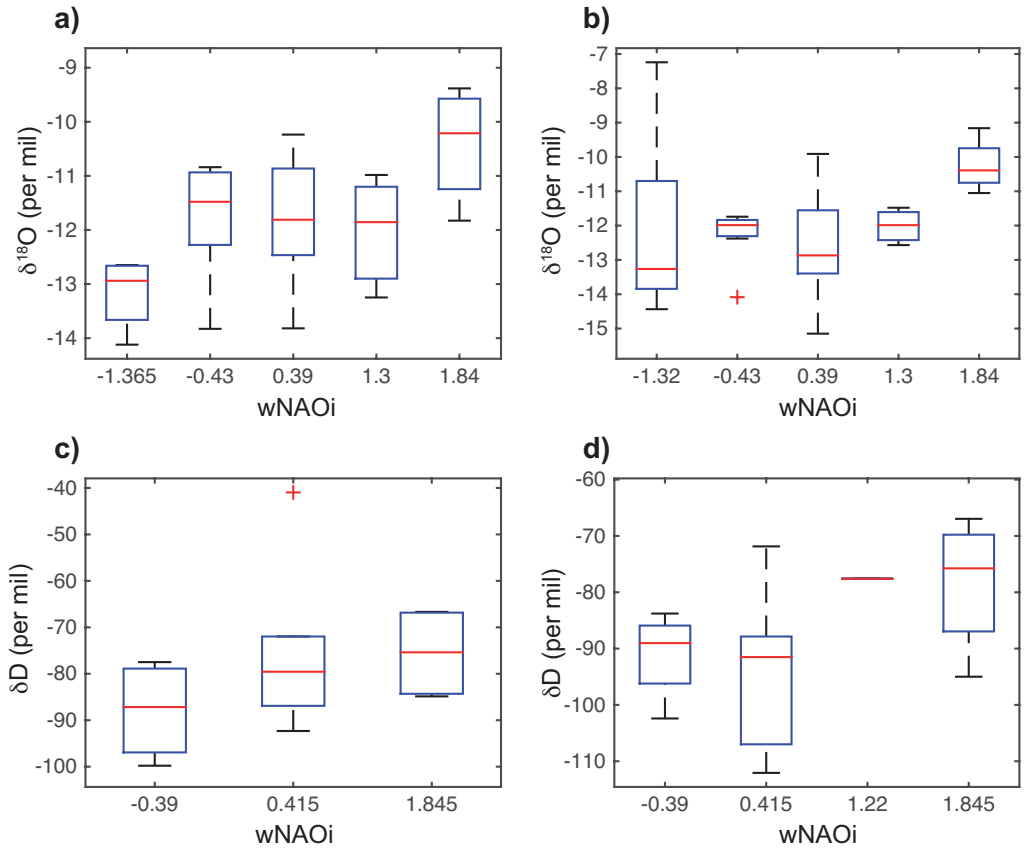

Station 16: Meiringen

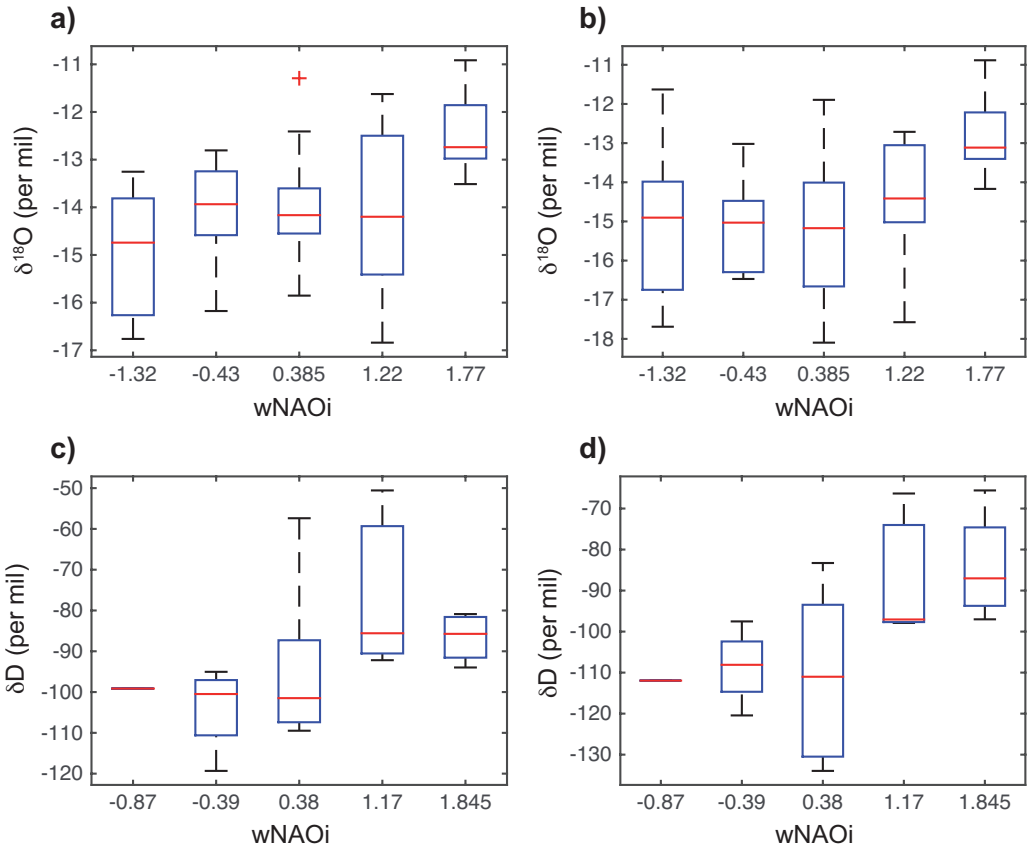

Station 17: Guttannen

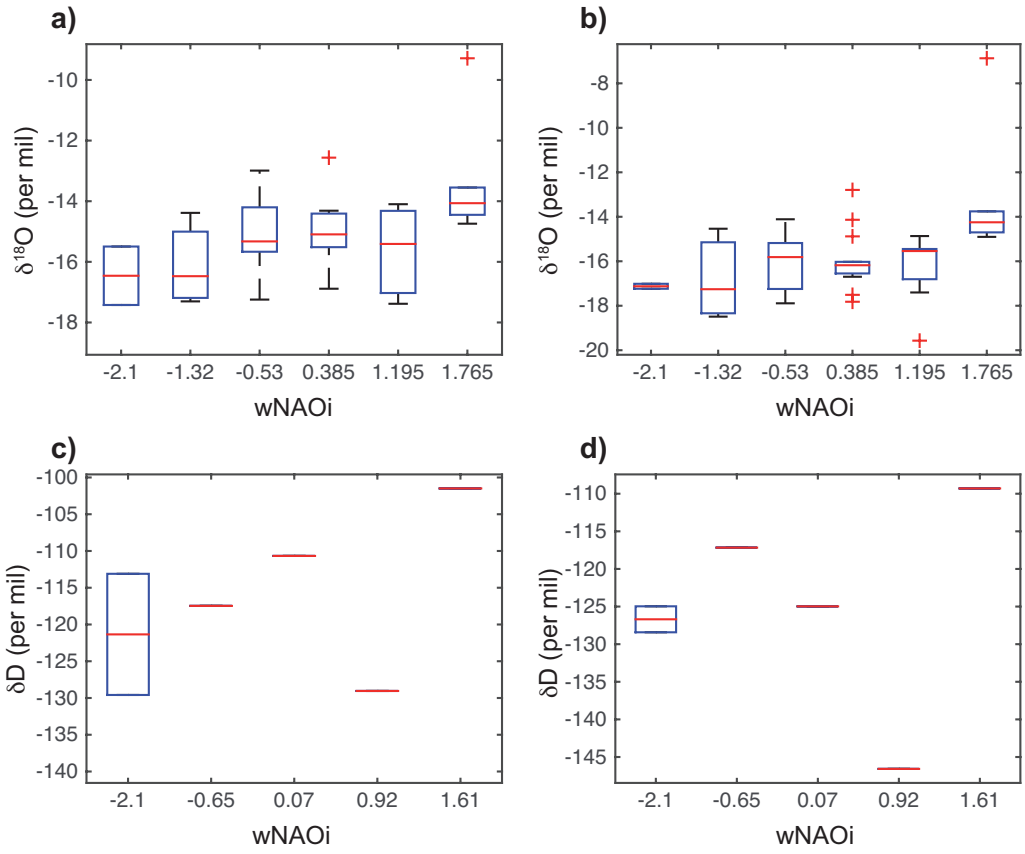

Station 18: Grimsel

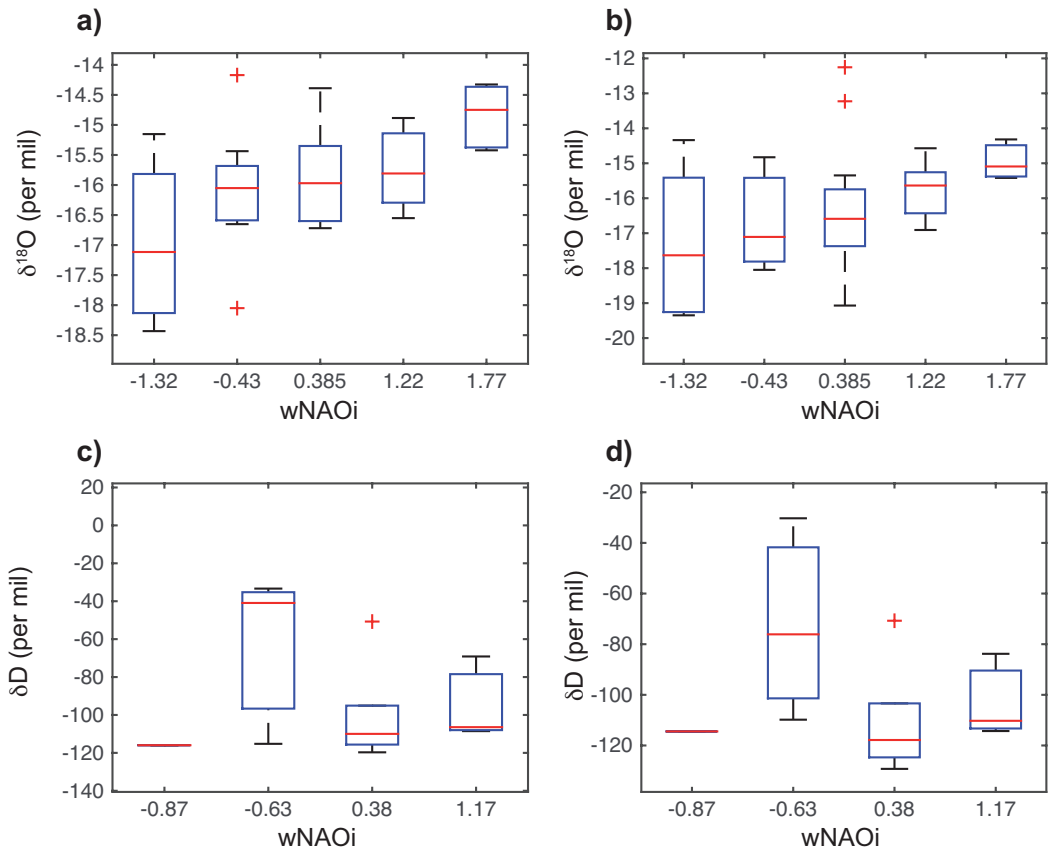

Station 19: Konstanz

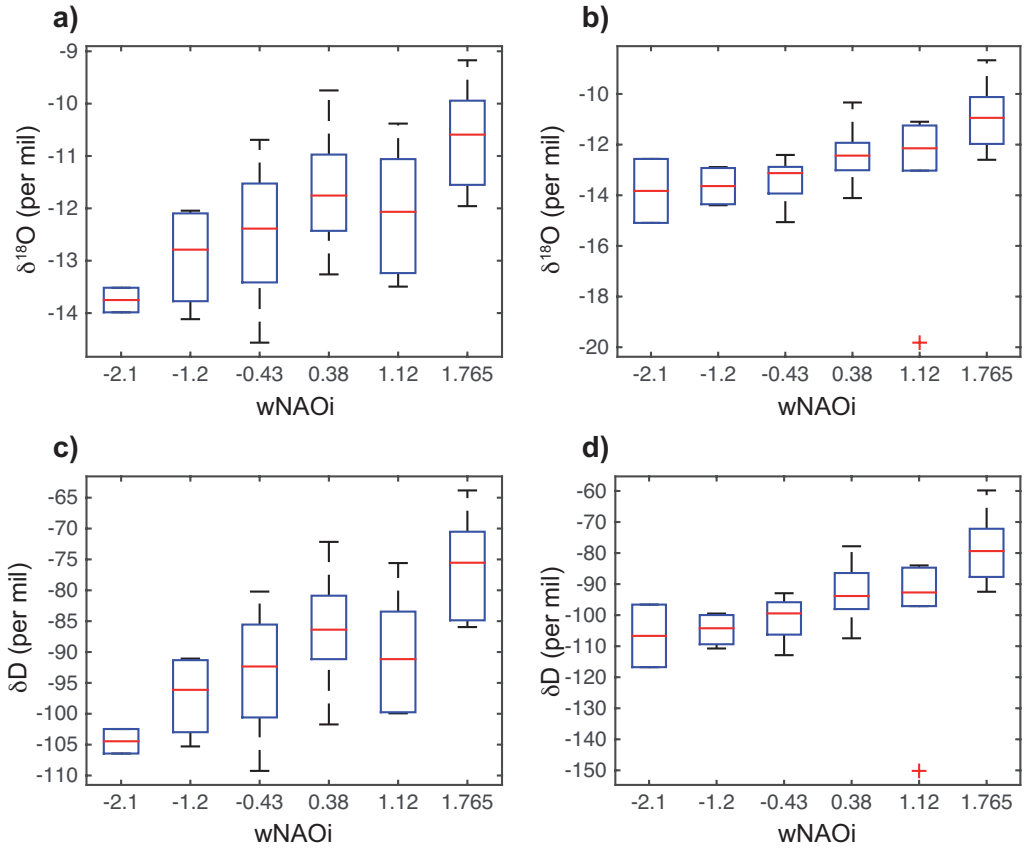

Station 20: Wasserkuppe Rhoen

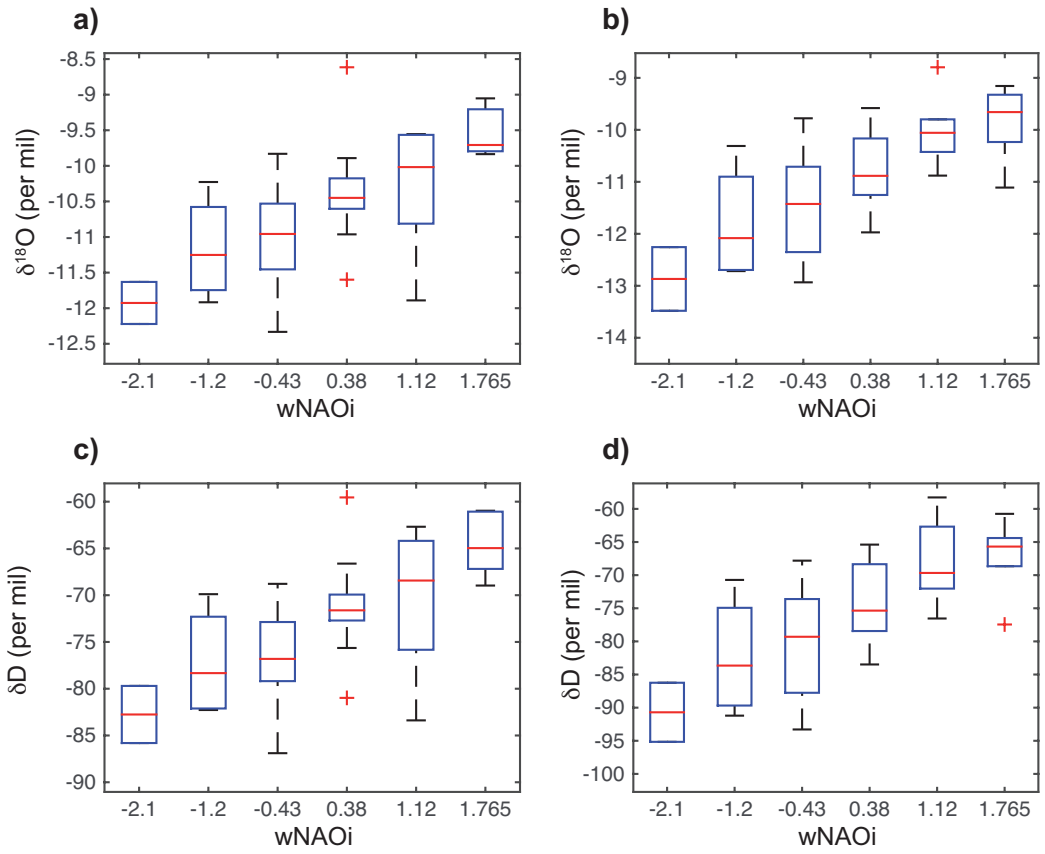

Station 21: Längenfeld

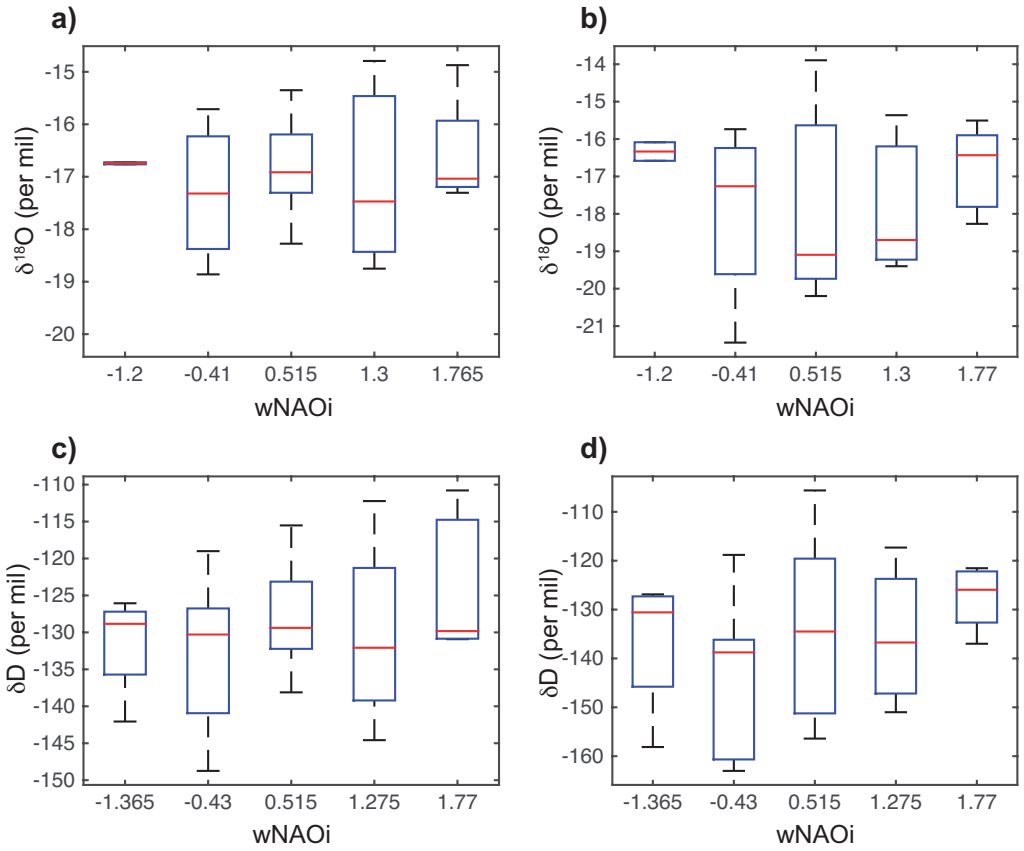

Station 22: Hohenpeissenberg

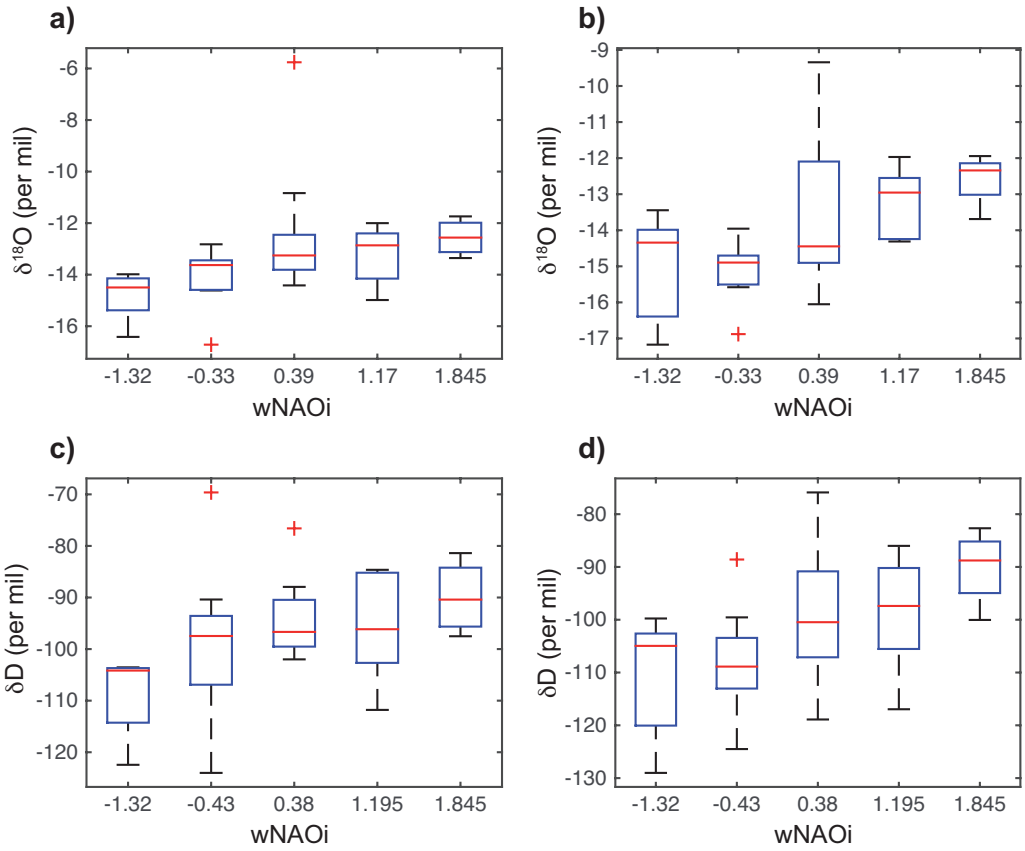

Station 23: Obergurgl

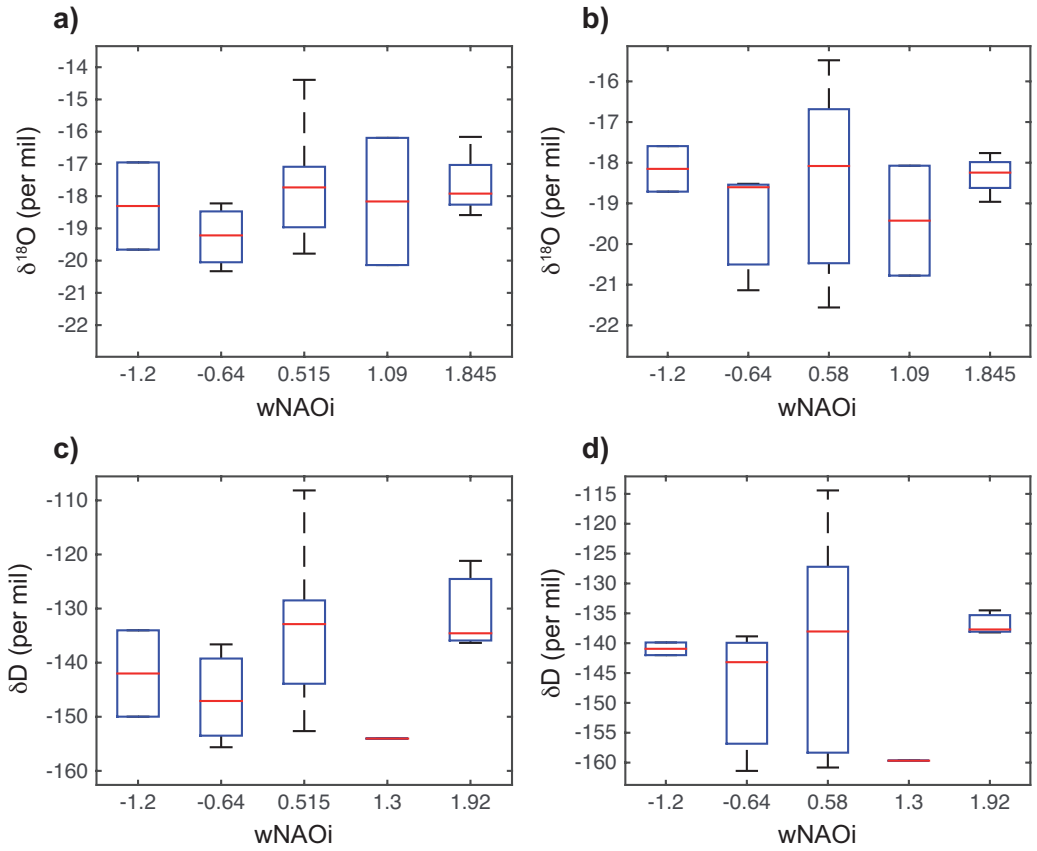

Station 24: Garmisch-Partenkirchen

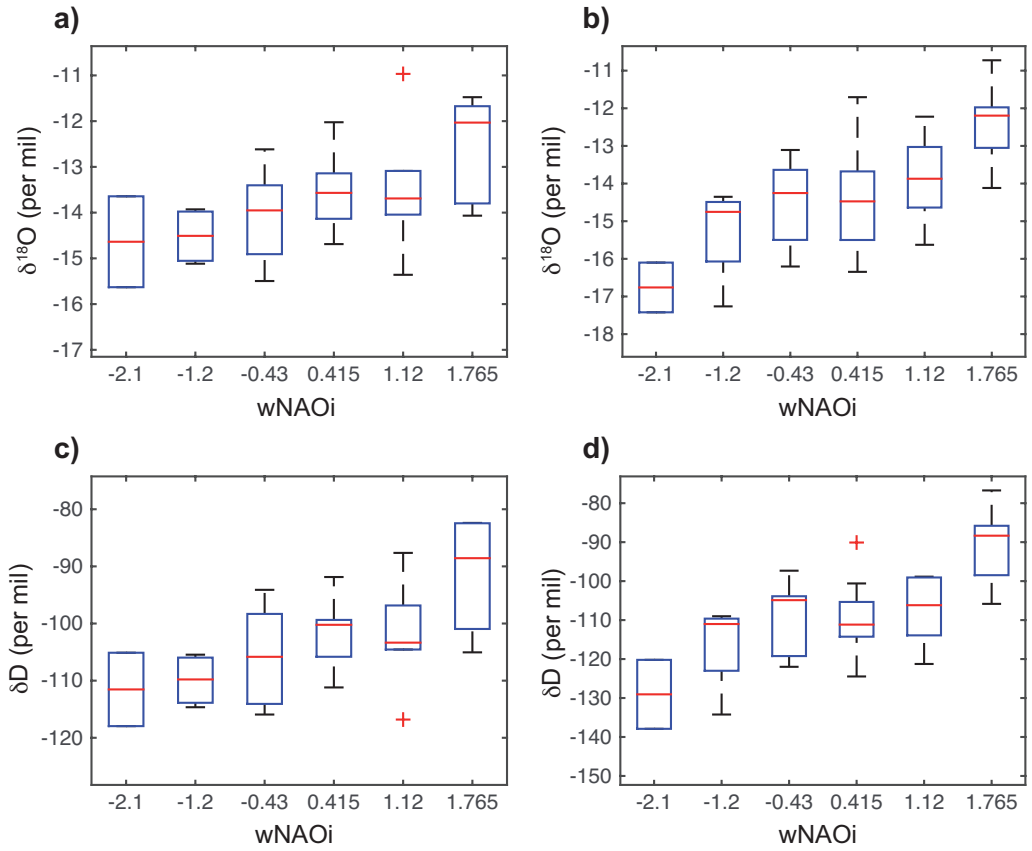

Station 25: Scharnitz

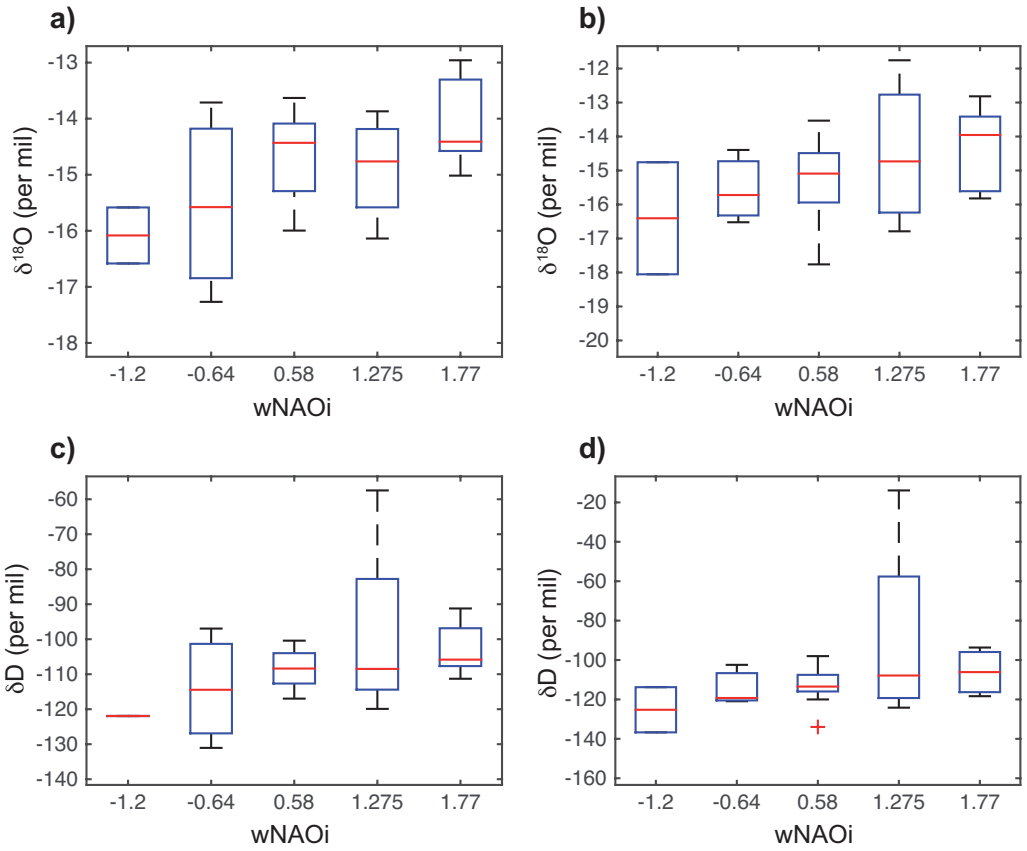

Station 26: Neuherberg

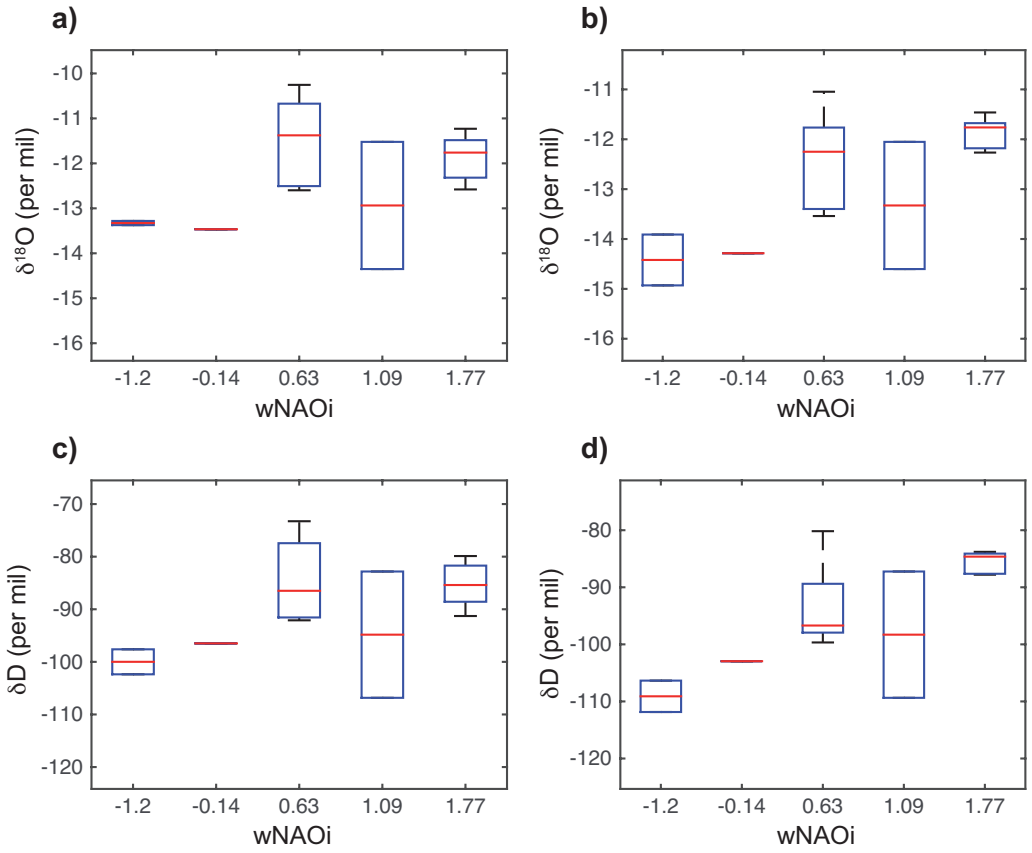

Station 27: Pastscherkofel

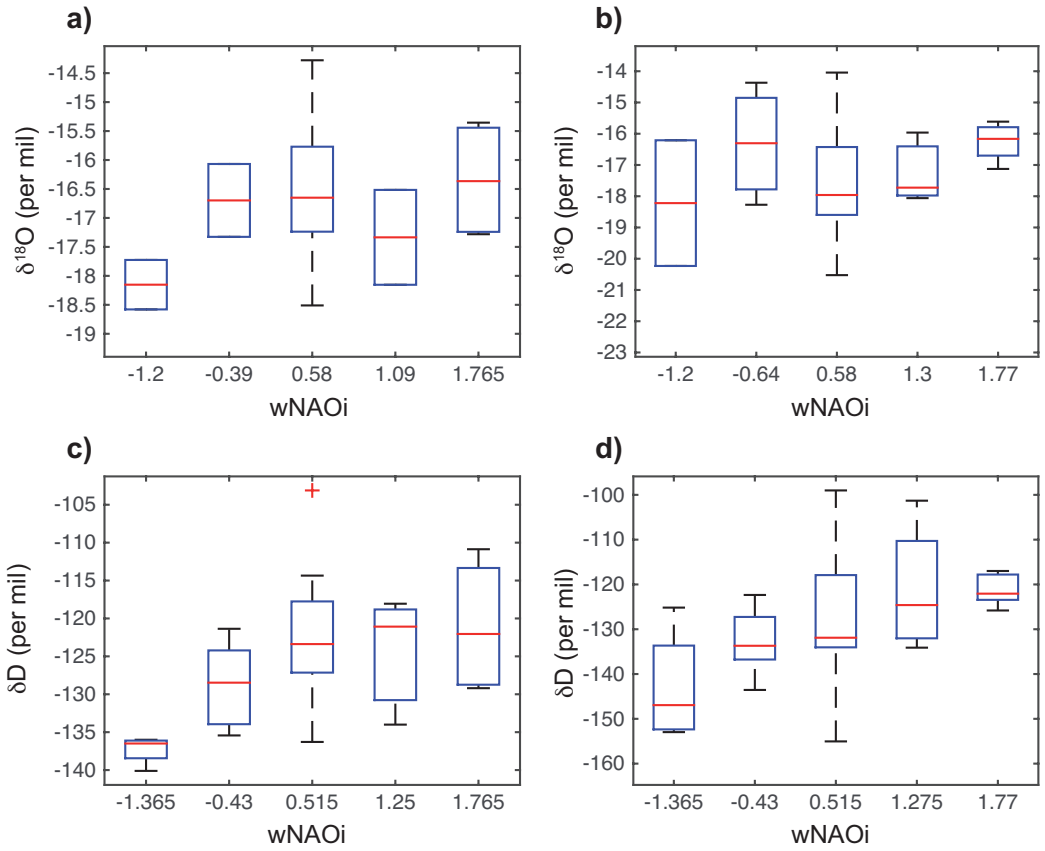

Station 28: Hof-Hohensaas

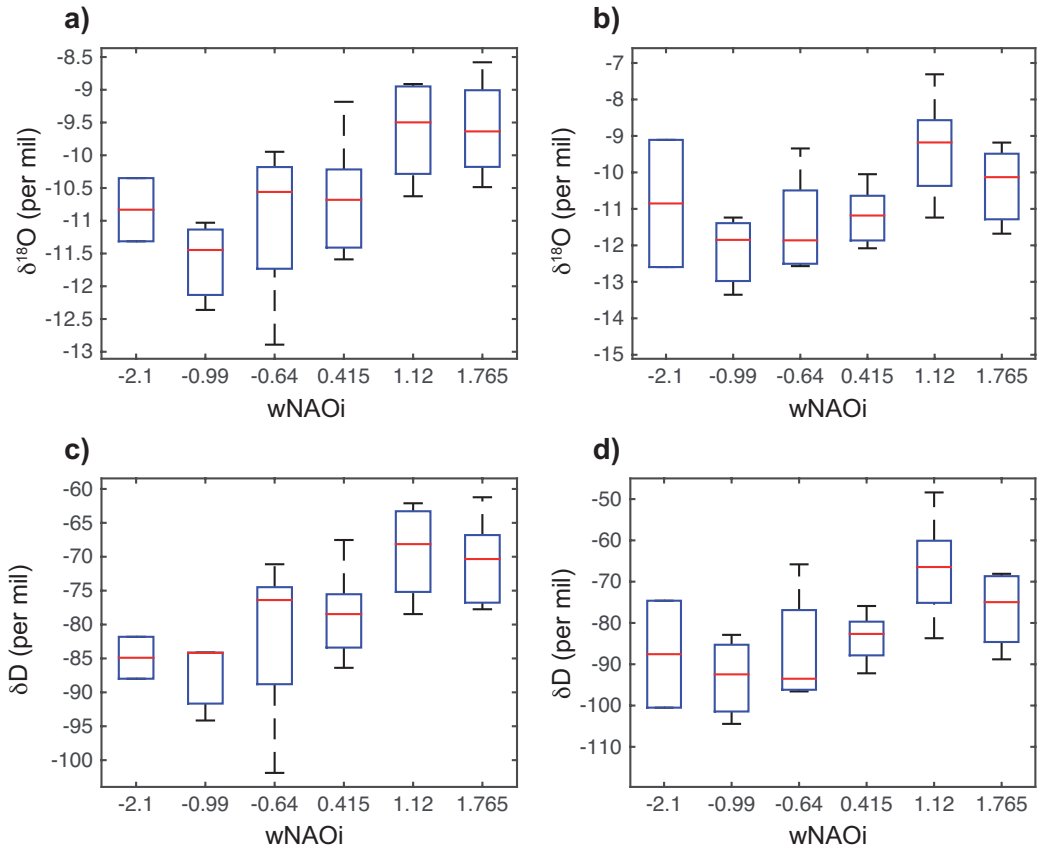

Station 29: Regensburg

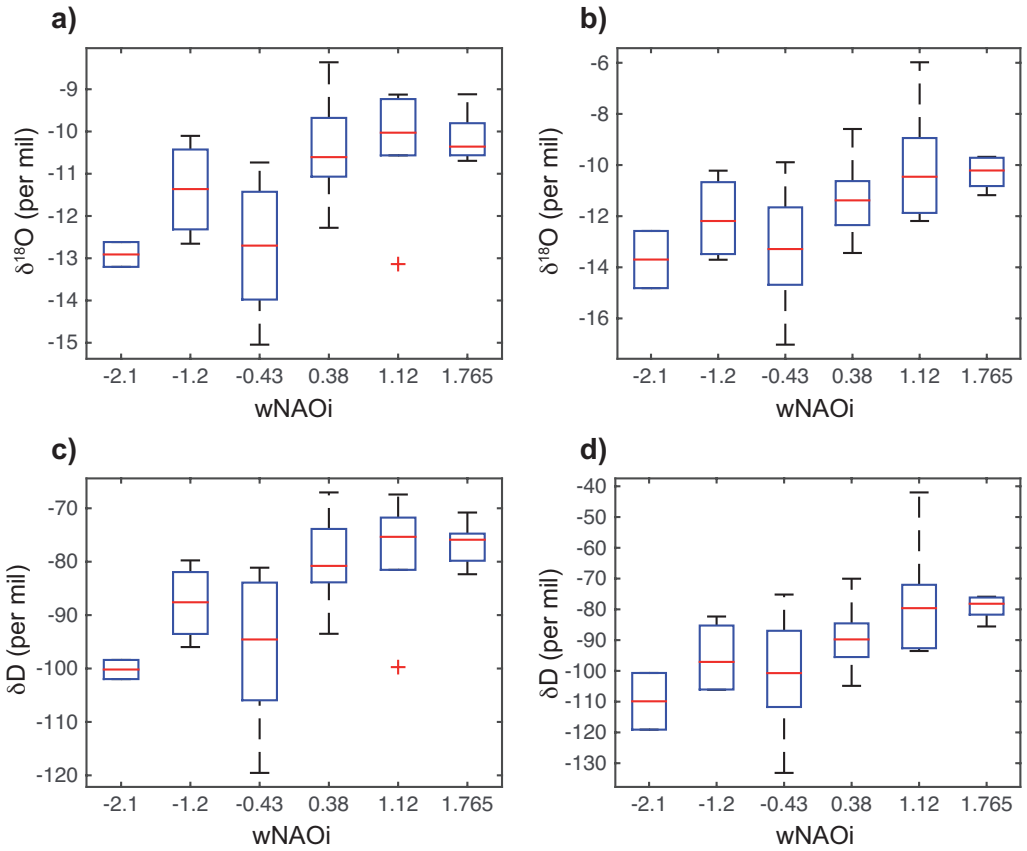

Station 30: Böckstein

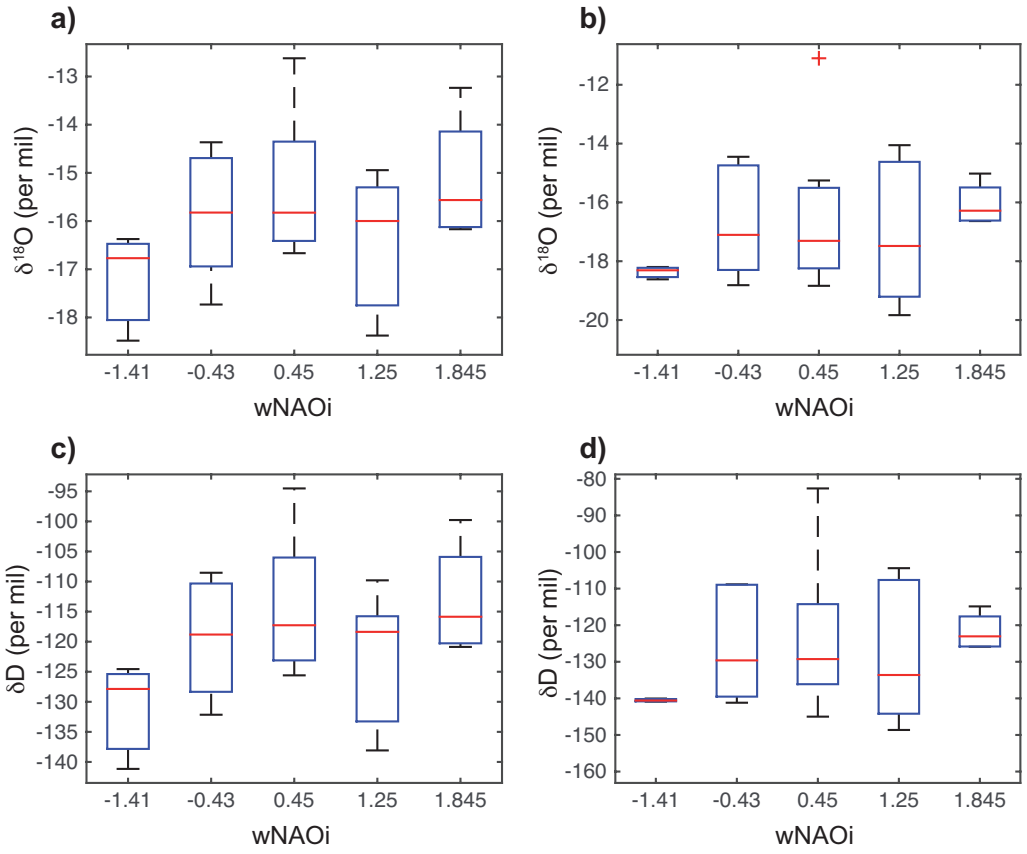

Station 31: St Peter

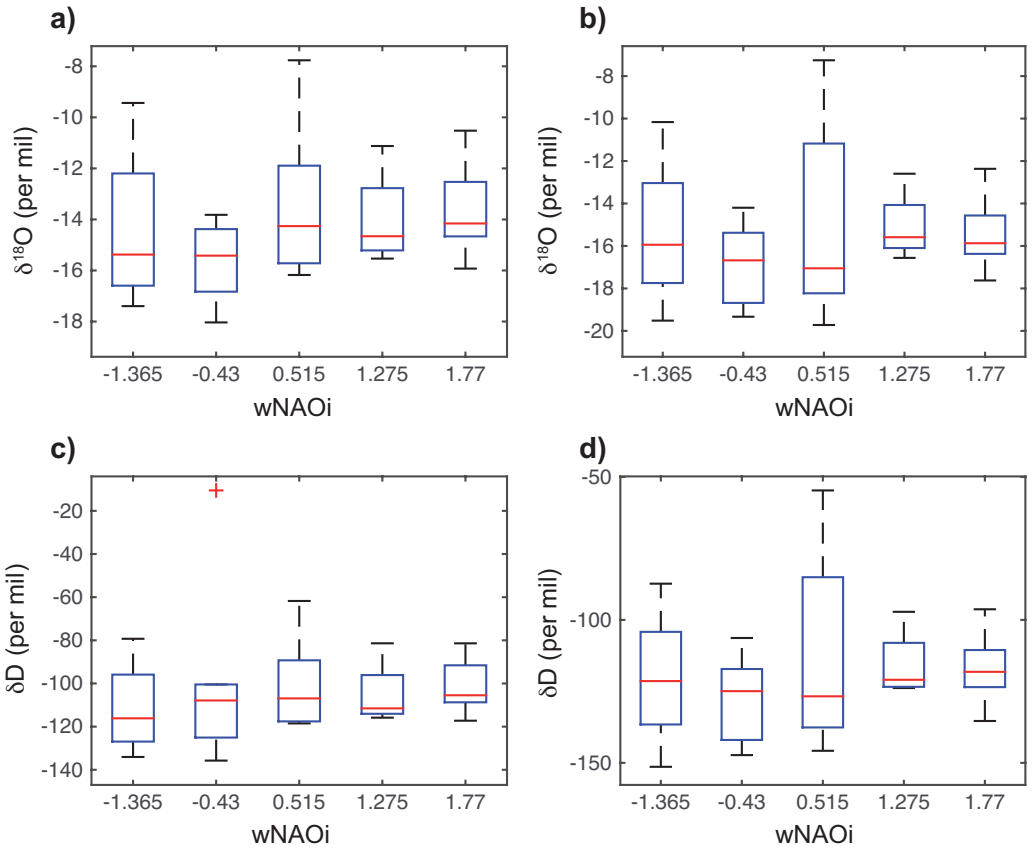

Station 32: Villacher Alpe

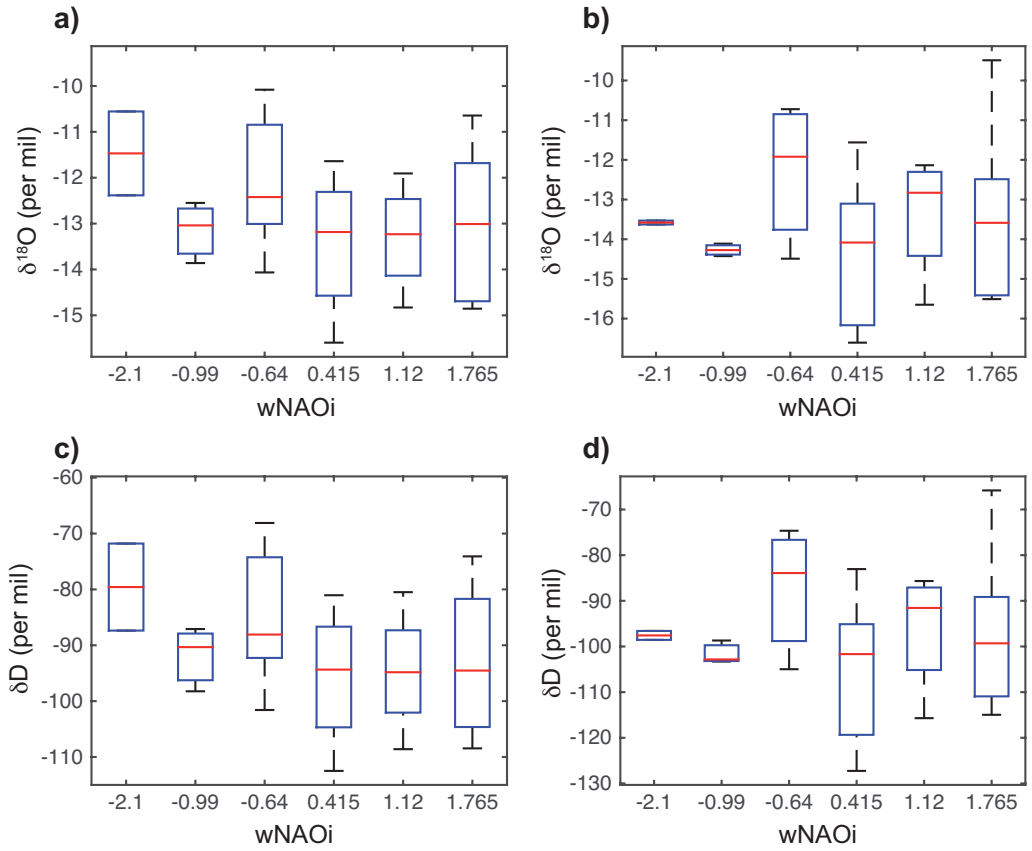

Station 33: Graz Universität

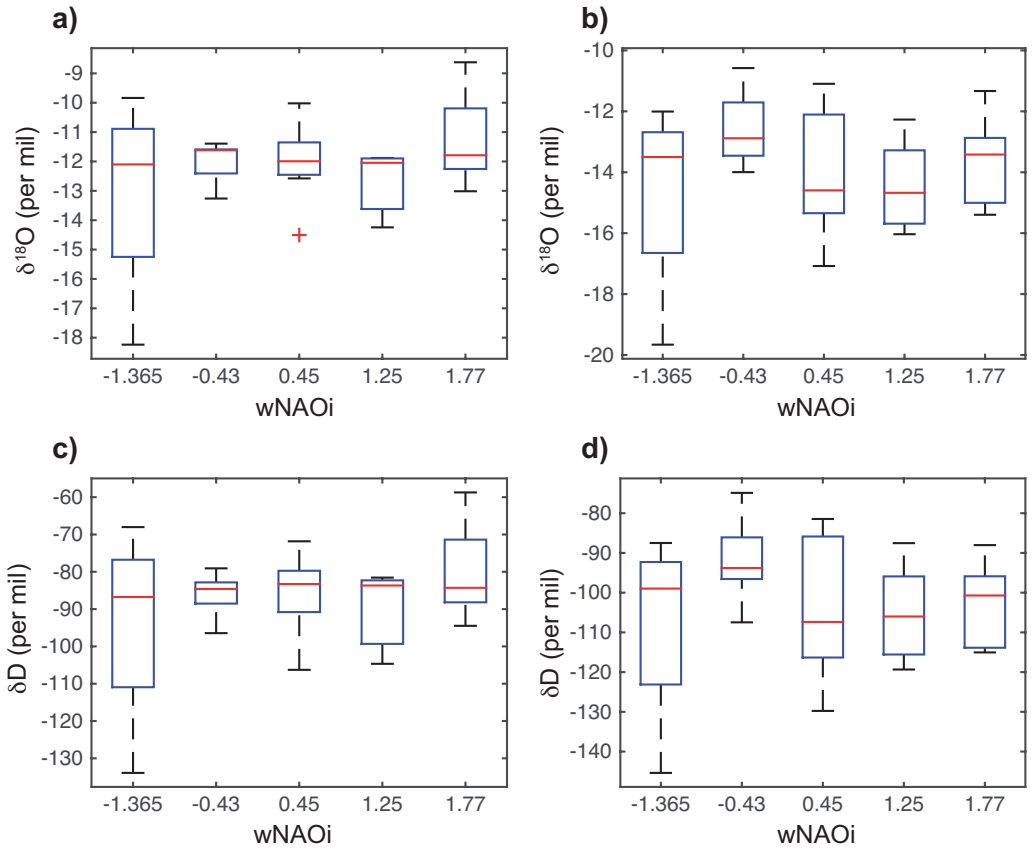

Station 34: Avignon

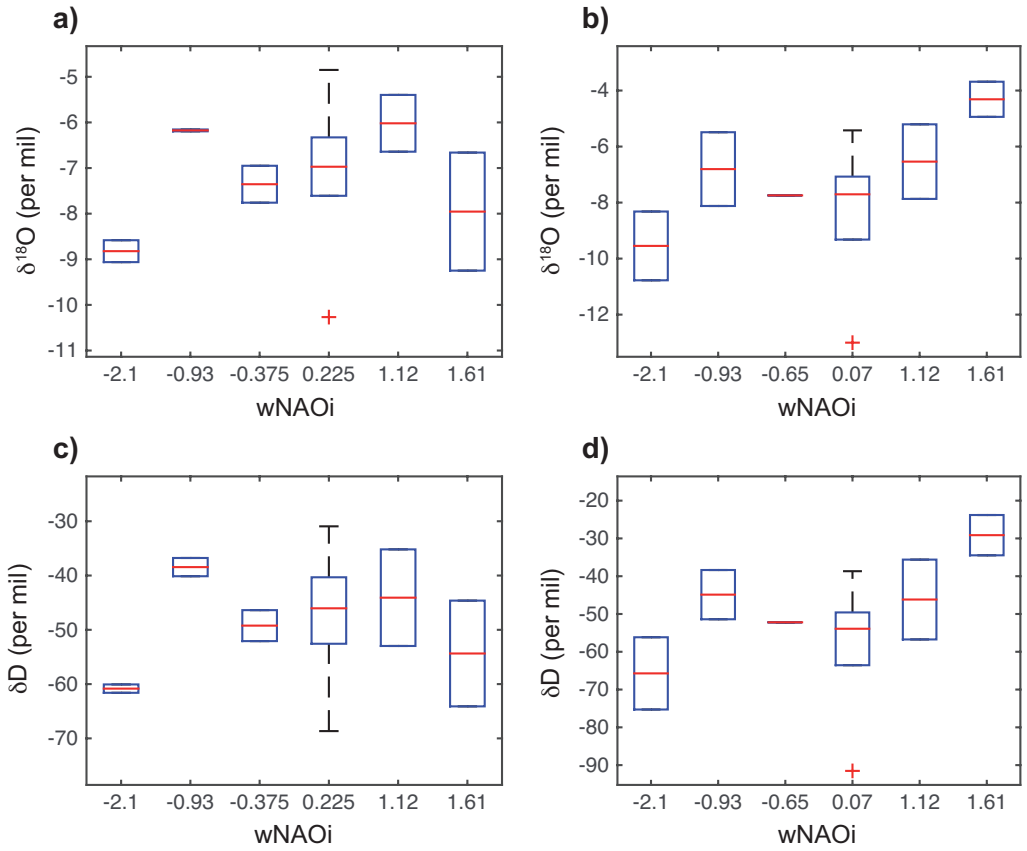

Station 35: Locarno

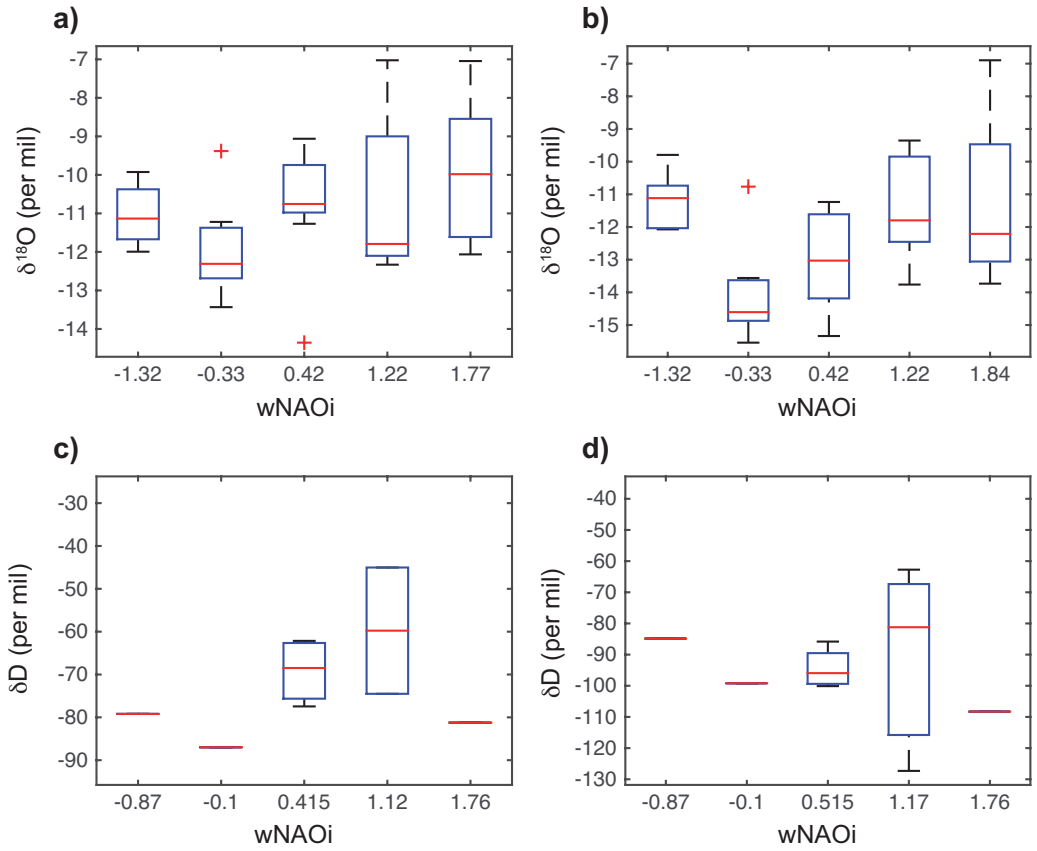

Station 36: Genoa (SESTRI)

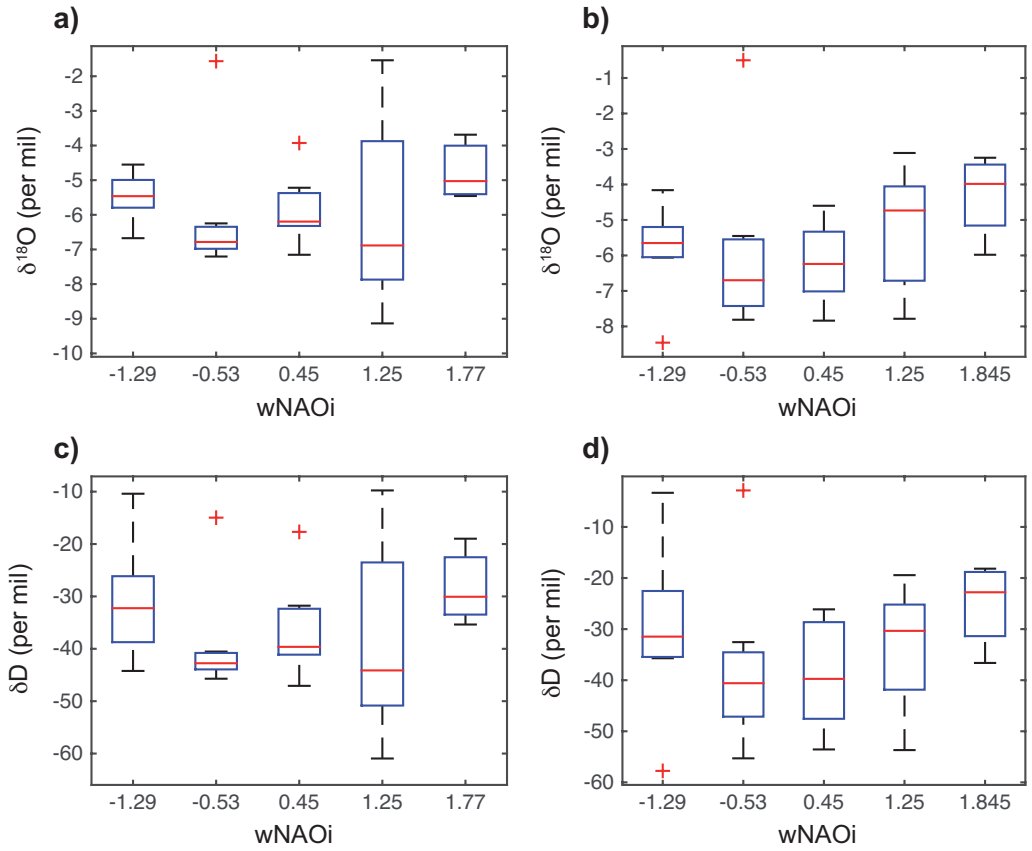

Station 37: Zagreb

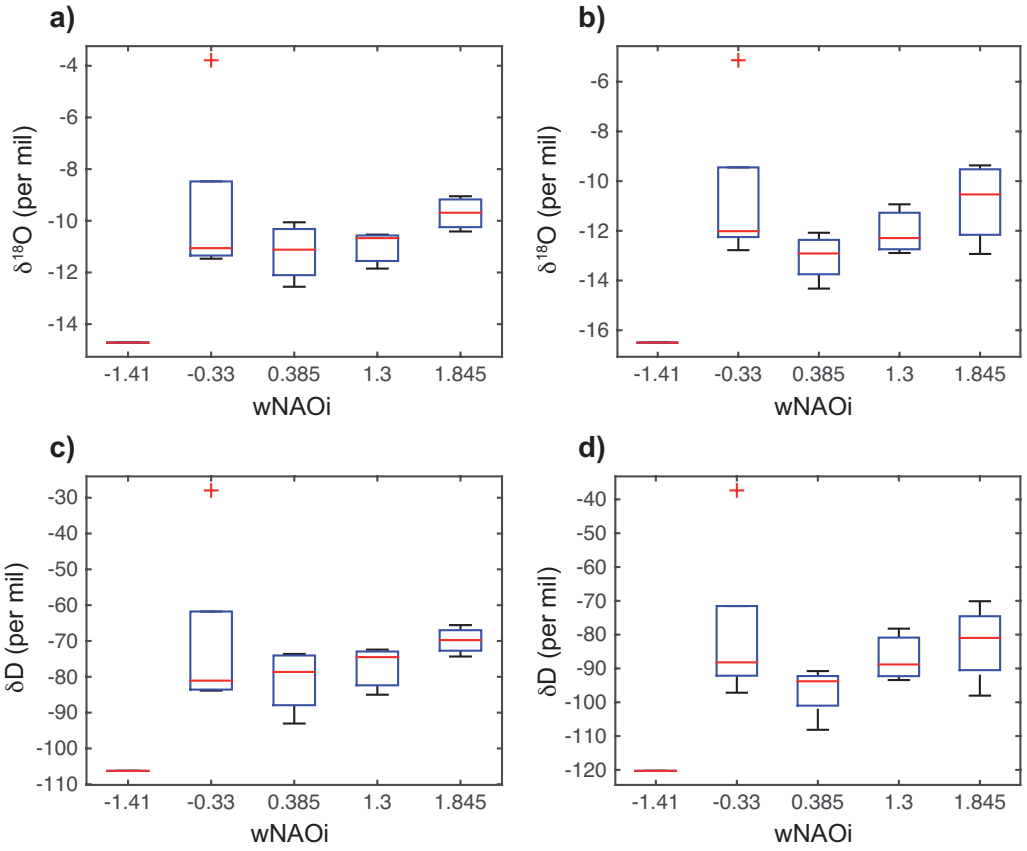

References:

Dansgaard, W.: Stable isotopes in precipitation, Tellus, 16, 436-468, 1964.
Langebroek, P. M., Werner, M., and Lohmann, G.: Climate information imprinted in oxygen-isotopic composition of precipitation in Europe, Earth and Planetary Science Letters, 2011.
Majoube, M.: Fractionnement en oxygene-18 et en deuterium entre l'eau et sa vapeur, J. Chim. phys, 68, 1423-1436, 1971.
Mook, W. G.: Introduction to isotope hydrology, Taylor & Francio, 8, 2006.
Trigo, R. M., Osborn, T. J., and Corte-Real, J. M.: The North Atlantic Oscillation influence on Europe: climate impacts and associated physical mechanisms, Climate Research, 20, 9-17, 2002.
Werner, M., Langebroek, P. M., Carlsen, T., Herold, M., and Lohmann, G.: Stable water isotopes in the ECHAM5 general circulation model: Toward high-resolution isotope modeling on a global scale, Journal of Geophysical Research, 116, D15109-D15109, 2011.